Methods for Very Long Baseline Atom Interferometry

Von der Fakultät für Mathematik und Physik der
Gottfried Wilhelm Leibniz Universität Hannover

zur Erlangung des Grades

Doktor der Naturwissenschaften
Dr. rer. nat.

genehmigte Dissertation von

Étienne Clément Wodey, M. Sc.

Hannover
2021

Referent
Prof. Dr. Ernst M. Rasel
Leibniz Universität Hannover
Institut für Quantenoptik

Korreferent
Prof. Dr. Wolfgang Ertmer
Deutsches Zentrum für Luft- und Raumfahrt e.V. (DLR)
Institut für Satellitengeodäsie und Inertialsensorik Hannover

Korreferent
Univ. Prof. Dr. Markus Arndt
Universität Wien
Fakultät für Physik

Vorsitzender der Prüfungskommission
Priv.-Doz. Dr. Hendrik Weimer
Leibniz Universität Hannover
Institut für Theoretische Physik

Tag der Promotion
9. Juli 2021

This document was typeset using LaTeX based on a template by Aurore Finco.
Document revision: d410d2.

Abstract

Gravity plays a central role in our understanding of the Earth and the Universe. It is the dominant force at astronomic scales, shaping star systems and galaxies. It is also a pivotal field in the geosciences, allowing access to the physical shape of the Earth, defining height systems, and tracking mass transport, for example water in climate change research, inside volcanoes, or along seismic faults. Finally, it could become a crucial resource for engineering, opening the way to a renewal of underground exploration techniques, both for natural resources and civil engineering legacy.

In fundamental physics, gravity nevertheless remains a riddle. From its origins to the first direct detection of gravitational waves in 2015, the theory of general relativity has accumulated successes. Our understanding of the microscopic world, through quantum mechanics and the standard model of particle physics is a similar success story, culminating with the detection of the BEH boson in 2012. Nevertheless, unification theories remain inaccessible and testing both the hypotheses and predictions of our theories remains the safest way towards the discovery of new physics. Here, key research areas relate to tests of the universality of free fall, at the heart of general relativity theory, or the creation of macroscopic superposition states of massive particles, a genuine marker of the quantum world.

Novel applications in the geosciences also require improved gravity sensors. For multiple applications in engineering and geodesy, the ideal device is easily transportable and has low energy consumption. Nevertheless, higher-order references are necessary to enable an accurate definition of a gravity standard across the world. Such gravity references could also be combined with state-of-the-art laser gyroscopes into quantum Earth observatories.

In this manuscript, we introduce a new generation of matter wave sensors based on very long baseline atom interferometry (VLBAI). Exploring the properties of massive quantum objects at the scales of meters and seconds, they will provide new insights into fundamental physics questions and serve as testbeds for novel atomic inertial sensors on ground and in space.

We provide the motivation and working principles for absolute gravity sensing with VLBAI, and discuss in particular the specific trade-offs arising from the use of an extended baseline in atom interferometry. We also present the core design of the Hannover VLBAI facility. Finally, we demonstrate that through a unique and carefully characterized 10 m-long magnetically shielded baseline, this devices offers the required environment for next-generation atomic gravity reference sensors and tests of fundamental physics.

Keywords: *large-scale matterwave interferometry, precision measurements, gravimetry*

Table of contents

1. Introduction

Cold atoms and ions are a versatile resource for many domains of modern physics. They lie at the core of modern quantum engineering, realizing quantum simulators and quantum computers. They also constitute a key element of state-of-the-art quantum metrology, producing the most precise frequency references,[1] contributing to the determination of fundamental constants,[2,3] and searching for new physics.[4] Furthermore, owing to the increased robustness and compactness of cold-atoms technology, even very large scale experiments and eminently challenging environments are accessible, including zero-g aircrafts, sounding rockets, and orbiting spacecrafts. All these developments aim at fully unleashing the potential of this promising technology and at providing reliable quantum-enhanced devices for scientific and consumer applications.[5]

Numerous key challenges nevertheless remain. While genuinely non-classical applications like *e.g.* quantum simulation or computing now reach unrivaled performance,[6] inertial sensing applications compete with but do not outperform significantly classical devices,[7] and certain key fundamental physics tests so far remain the undisputed domain of classical instruments.[8] Cold atoms-based devices however have distinct advantages over classical counterparts: simple and perfectly reproducible physical systems, excellent understanding of their interactions, good decoupling from their environment, versatility of measurement geometries, and even the possibility of an increased scale factor[9] or improved noise performance[10] due to the emergence of quantum properties.

To further investigate Earth-bound precision atom interferometry, we started in 2014 the construction of the Hannover Very Long Baseline Atom Interferometry (VLBAI) facility, a major research instrument that will serve as a testbed for both the science and the technology of future atom interferometers. With its 10 m-scale vertical baseline, it supports research programs targeting geodetic metrology, detection of gravitational waves

[1] A. D. Ludlow et al. *Rev Mod Phys* 87, 637 (2015) [1]

[2] L. Morel et al. *Nature* 588, 61 (2020) [2]

[3] G. Rosi et al. *Nature* 510, 518 (2014) [3]

[4] M. S. Safronova et al. *Rev Mod Phys* 90, 025008 (2018) [4]

[5] M. Travagnin. *JRC Tech Rep*, EUR 30492 (2020) [5]

[6] K. Wright et al. *Nat Commun* 10, 5464 (2019) [6]

[7] P. Gillot et al. *Metrologia* 51, L15 (2014) [7]

[8] P. Touboul et al. *Phys Rev Lett* 119, 231101 (2017) [8]

[9] H. Müller et al. *Phys Rev Lett* 100, 180405 (2008) [9]

[10] F. Anders et al. (2020). arXiv: 2010.15796 [10]

in the infrasound domain, tests of fundamental physics, as well as searches for new physics at the interface between quantum mechanics and general relativity through, *e.g.*, the investigation of macroscopic quantum superpositions and quantum clocks. Meanwhile, other large-scale projects have been started, such as the Matter wave laser-Interferometric Gravitational Antenna MIGA[11] in France, the Atom Interferometer Observatory and Network AION[12] in the United Kingdom, and the Matter wave Atomic Gradiometer Interferometric Sensor MAGIS[13] in the USA. Pioneering instruments, like for example the one at Stanford University (USA), also recently delivered their first metrologically significant results.[14] This shows the vitality of this research field as a complementary path to expensive and technologically more demanding micro-gravity missions to explore atom interferometry on long timescales and large distances.

Here, we describe the early development work of the Hannover VLBAI facility. Based on the example of absolute atomic gravimetry, we illustrate and discuss the key requirements and design trade-offs for our 10 m-scale instrument. Absolute atomic gravimetry is particularly relevant since it is a distinctive target of the Hannover VLBAI facility when compared to other instruments worldwide which focus on differential measurements, for example towards the detection of infrasound gravitational waves and dark-matter searches (MAGIS, AION) or tests of the universality of free fall (Stanford, Wuhan). Large-scale atomic gravimeters nonetheless have the potential to go beyond the current state of the art formed by falling corner cube and superconducting devices[15] by offering the resolution of superconducting meters while providing absolute measurements. In the future, they could constitute higher-order references for transportable field instruments. Also, their combination with atomic clocks,[16] large-scale laser gyroscopes,[17] and horizontal atomic gradiometers[18] could form quantum geodetic observatories to improve our understanding of the Earth's gravity field.[19]

This manuscript is organized around multiple peer-reviewed publications stemming from the research performed to motivate, design, and realize the VLBAI facility and its three major components: high-flux sources of ultracold ytterbium and rubidium atoms, an in-vacuum vibration-isolated inertial reference to enable absolute measurements, and the 10 m-long, magnetically shielded, ultra-high vacuum chamber that hosts the atom interferometer's baseline. Chapter 2 briefly recaps the basics of atomic gravimetry and introduces the key equations guiding accuracy and noise considerations for atom-interferometric gravimeters. Noise and aliasing mitigation is in particular the

[11] B. Canuel et al. *Sci Rep* 8, 14064 (2018) [11]

[12] L. Badurina et al. *J Cosmol Astropart P* 5, 11 (2020) [12]

[13] M. Abe et al. (2021). arXiv: 2104.02835 [13]

[14] P. Asenbaum et al. *Phys Rev Lett* 125, 191101 (2020) [14]

[15] I. Marson et al. *J Phys E: Sci Instrum* 19, 22 (1986) [15]

[16] J. Grotti et al. *Nat Phys* 14, 437 (2018) [16]

[17] K. U. Schreiber et al. *Pure Appl Geophys* 166, 1485 (2009) [17]

[18] B. Canuel et al. *Sci Rep* 8, 14064 (2018) [11]

[19] M. Van Camp et al. *Rev Geophys* 55, 938 (2017) [18]

motivation for our work on a high-flux source of cold ytterbium atoms:

E Wodey et al., A robust, high-flux source of laser-cooled ytterbium atoms, J Phys B: At Mol Opt 54, 035301 (2021).

In chapter 3, we dive into some of the fundamental changes arising from the fifty-fold increase in baseline length compared to transportable atomic and classical instruments. Beyond atom-optics and engineering challenges, 10 m-scale atom-interferometric gravimeters enter domains where the control of the instrument's effective height at the required millimeter-level becomes challenging, and anharmonicities of the gravitational potential systematically modify the interferometric phase.[20] We provide a quantitative analysis of the effect of gravity variations along the baseline based on our model of the static gravity profile and first dynamic corrections for the Hannover VLBAI facility:

[20] P. Asenbaum et al. *Phys Rev Lett* 118, 183602 (2017) [19]

M Schilling, **E Wodey** et al., Gravity field modelling for the Hannover 10 m atom interferometer, J Geodesy 94, 122 (2020).

Furthermore, the increase in scale factor provided by the extended baseline also implies an increased sensitivity to vibrations of the instrument's inertial reference. We show that an in-vacuum, geometric anti-spring-based seismic attenuation platform provides a good starting point for VLBAI gravimetry but is not sufficient to utilize the technology's full potential. Hybridization with classical high-bandwidth sensors[21] is necessary to mitigate aliasing and potentially obtain best sensitivities. In the long-term, the use of genuinely vacuum-compatible, ultra-compact optical sensors will significantly enhance inertial reference platforms for VLBAI facilities, as described in our pioneering work:

[21] J. Lautier et al. *Appl Phys Lett* 105, 144102 (2014) [20]

L L Richardson, ..., **E Wodey** et al., Optomechanical resonator-enhanced atom interferometry, Commun Phys 3, 208 (2020).

Moving away from general considerations, chapter 4 provides technical insight into the design of the VLBAI facility's baseline hardware. We demonstrate that careful engineering allows to constrain the environmentally-induced systematic effects better than 1 nm/s^2 acceleration bias. One major achievement, and cornerstone of the instrument, is its 10 m-long high-performance magnetic shield, described in detail in our article:

E Wodey et al., A scalable high-performance magnetic shield for very long baseline atom interferometry, Rev Sci Instrum 91, 035117 (2020).

We conclude this manuscript by briefly reviewing other applications of large-scale atom interferometers that enter the Hannover facility's research agenda. This includes in particular prospects for enhanced atomic tests of the universality free fall[22] and highly de-localized quantum clocks, a concept described in detail in our study on an atom-interferometric realization of the famous twin paradox:

[22] J. Hartwig et al. *New J Phys* 17, 035011 (2015) [21]

S Loriani, ..., **E Wodey** et al., Interference of clocks: A quantum twin paradox, Sci Adv 5, eaax8966 (2019).

The Hannover VLBAI facility is a major research instrument funded by the German Science Foundation (Deutsche Forschungsgemeinschaft, DFG) and implemented in the Hannover Institute of Technology (**HITec**) of the Leibniz University Hannover. The DFG collaborative research centers (Sonderforschungsbereich, SFB) 1128 "**geo-Q**" and 1464 "**TerraQ**" aim at developing the research linked to geodetic applications of quantum sensors. The CRC 1227 "**DQ-mat**" supports the study and implementation of the concept of quantum clocks and the research agenda on fundamental physics. Finally, the DFG excellence cluster 2123 "**QuantumFrontiers**" as well as Lower Saxony's "**QUANOMET**" initiative provide the framework for the development of applied and fundamental quantum technologies in the Hannover–Braunschweig region.

2. Atom-interferometric gravimetry

Terrestrial gravimeters are instruments that measure the acceleration of a massive test body in the gravitational field of the Earth in order to determine the acting gravitational force. One can distinguish two types of gravimeters. On one hand, relative instruments link the test body's acceleration to an instrument-dependent artifact, for example a spring constant for spring gravimeters or electromagnetic fields for superconducting gravity meters. On the other hand, absolute gravimeters aim at measuring the gravity value directly in SI units, ideally reproducing the ideal Newtonian experiment: a massive body in free fall, whose acceleration is measured in the Galilean reference frame of the Earth. Instruments from both categories have advantages and drawbacks. Relative gravimeters offer in general significantly higher sampling rates. Spring gravimeters are also highly transportable as the full instruments fits in a few liters package. Superconducting gravimeters are bulkier but feature outstanding sensitivities[1] and can run with no interruptions for decades.[2]

The gold standard in absolute gravimetry is the free-falling corner cube gravimeter. In such instruments, a laser interferometer records the free fall of a corner cube reflector with respect to another one mounted on a so-called super-spring isolator that forms the inertial reference.[3] In modern Micro-g Lacoste FG5-X instruments, a Mach-Zehnder laser interferometer records more than 1000 samples of the corner cube's position along its approximately 30 cm free-fall trajectory.[4] A least-squares adjustment based on the expected trajectory is then performed to extract the local gravitational acceleration g. Such instruments have been successfully used in numerous absolute gravimetry campaigns.[5] Comparison studies have constrained their inaccuracy to around 10 $\mathrm{nm/s^2}$.[6]

Atomic gravimeters realize an experiment similar to the falling corner cube instruments, however replacing macroscopic glass

[1] J. M. Goodkind. *Rev Sci Instrum* 70, 4131 (1999) [22]

[2] M. Van Camp et al. *Eos* 98 (2017) [23]

[3] T. M. Niebauer et al. *Metrologia* 32, 159 (1995) [24]

[4] Samples at the beginning and the end of the trajectory are usually discarded. The exact number of used samples can be configured by the operator.

[5] M. Bilker-Koivula et al. *J Geodesy* 95, 24 (2021) [25]

[6] V. Pálinkáš et al. *J Geodesy* 95, 21 (2021) [26]

artifacts by atomic ensembles as their test masses. Specifically cold atoms display interesting features that make them close-to-ideal test masses. First their small spatial extent makes it easier to control the surrounding environment. Also, laser cooling produces dilute and isotopically pure atomic samples, such that interactions within and outside the sample are simply described and understood in comparison to solid-state systems. Finally, low temperatures correspond to large de Broglie wavelengths and low velocity dispersions, thus rendering the wave-like nature of atomic particles more prominent and enabling efficient interferometric techniques to augment measurement sensitivities.

Following the introduction of the atomic equivalent of the optical Mach-Zehnder interferometer,[7] Peters *et al* presented in 2001 a cesium-based instrument with a sensitivity of $30\,\mathrm{nm/s^2/\sqrt{Hz}}$ after one minute and a similar-scale accuracy,[8] thus already competing with falling corner cube devices. Transportable atomic gravimeters, like the CAG from the French national metrology laboratory LNE-SYRTE in Paris[9] and GAIN from the Humboldt University in Berlin,[10] have received considerable attention by participating in key comparison campaigns and field surveys respectively. This was the result of careful characterization and modeling of their systematic effects, that lead to robust error budgets with accuracies around $40\,\mathrm{nm/s^2}$.

Numerous challenges nevertheless remain for atomic gravimeters to significantly transform the field of absolute gravimetry. On the one hand, the reliability and usage simplicity need to be highly increased to accommodate the extreme conditions reigning at relevant measurement sites. In this direction, the French company Muquans recently deployed a commercial cold-atoms gravimeter on Mount Etna to monitor its volcanic activity, as part of the international collaboration Newton-g.[11] On the other hand, the question remains open whether cold-atoms-based instruments can achieve sub $1\,\mathrm{nm/s^2}$ accuracy. This level is where random and systematic errors due to uncertainties in e.g. tidal reduction models start to be significant and the disentangling between signal of interest and unwanted noise is challenging.[12] Significant effort is currently put into existing[13] and novel[14] devices to enter this domain and provide relevant accuracy evaluations.

In this chapter, we review the basics of atomic gravimeters and present the key equations governing their sensitivity. These will serve as the motivation for very long baselines, as discussed in chapter 3. The analysis of raw data from absolute gravimeters requires a model for the gravitational field. In section 2.1, we briefly derive the simplest non-trivial model that takes into account the normal change of gravity with height. Subsequently,

[7] M. A. Kasevich et al. *Phys Rev Lett* 67, 181 (1991) [27]

[8] A. Peters et al. *Metrologia* 28, 25 (2001) [28]

[9] P. Gillot et al. *Metrologia* 51, L15 (2014) [7]

[10] C. Freier et al. *J Phys: Conf Ser* 723, 012050 (2016) [29]

[11] D. Carbone et al. *Front Earth Sci* 8, 573396 (2020) [30]

[12] J. E. Faller. *Metrologia* 39, 425 (2002) [31]

[13] R. Karcher et al. *New J Phys* 20, 113041 (2018) [32]

[14] N. Heine et al. *Eur Phys J D* 74, 174 (2020) [33]

we introduce the main concepts and key results of generic light-pulse atom interferometry (section 2.2) and finally discuss the ubiquitous Mach-Zehnder-like geometry (section 2.3) and the fundamental limits to its measurement stability (section 2.4).

2.1. Trajectories in the Earth gravity field

We consider the Earth as a spherical body of radius $R_\oplus$ and mass $M_\oplus$. The gravitational potential of a test mass m at an altitude z above the Earth's surface reads:

$$V(z) = -\frac{GmM_\oplus}{R_\oplus + z} \tag{2.1}$$

where $G \approx 6.67 \times 10^{-11}\,\mathrm{m^3/(kg\,s^2)}$ is the Newtonian gravitational constant. The acceleration on the test mass m is independent of m (equivalence principle) follows by derivation:

$$g(z) = -\frac{GM_\oplus}{R_\oplus^2}\frac{1}{\left(1+\frac{z}{R_\oplus}\right)^2} = -\frac{GM_\oplus}{R_\oplus^2}\left(1 - 2\frac{z}{R_\oplus} + \mathcal{O}\left(\frac{z}{R_\oplus}\right)^2\right). \tag{2.2}$$

This is the simplest non-uniform static gravity model for the Earth. We identify the well-known gravitational acceleration

$$g_0 = \frac{GM_\oplus}{R_\oplus^2} \approx 9.8\,\mathrm{m/s^2} \tag{2.3}$$

and the free-air gradient, which corresponds to the linear change of gravity with height:

$$\gamma_0 = \frac{2GM_\oplus}{R_\oplus^3} \approx 3.1\,\mathrm{\mu m/s^2/m}. \tag{2.4}$$

The truncation of the quadratic terms leads to an error on the order of $10\,\mathrm{nm/s^2}$ at $z = 100\,\mathrm{m}$.

Since every massive body contributes to the gravitational acceleration of the test mass m, extensions of this model are numerous. Significant static corrections stem from the density of the local ground, nearby mountains or buildings, etc. The most well-known dynamic corrections are the lunar and solar tides, with a total amplitude around $2\,\mathrm{\mu m/s^2}$. More locally, mass transport phenomena, like for example seasonal or episodic

ground-water level variations or even magma movements in volcanic cones contribute at the few 10 nm/s^2 level and constitute some of the major application targets of terrestrial gravimetry.[1]

[1] D. Carbone et al. *Front Earth Sci* 8, 573396 (2020) [30]

The equation of motion for the test mass m in the field modeled by equation 2.2 follows from Lagrangian theory:

$$\ddot{z} - \gamma_0 z = -g_0 \tag{2.5}$$

which is a simple polynomial differential equation whose solution for initial position z_0 and velocity v_0 is[2]

[2] A. Peters et al. *Metrologia* 28, 25 (2001) [28]

$$z(t) = \frac{g_0}{\gamma_0} + \left(z_0 - \frac{g_0}{\gamma_0}\right) \cosh\left(\sqrt{\gamma_0} t\right) + \frac{v_0}{\sqrt{\gamma_0}} \sinh\left(\sqrt{\gamma_0} t\right). \tag{2.6}$$

The quantity $\gamma_0 \Delta t^2$ is dimensionless and quantifies the fractional change of gravity experienced by the test body m in an experiment of duration Δt. Free fall experiments on the Earth's surface typically last at most a few seconds, such that $\gamma_0 \Delta t^2 \approx 1 \times 10^{-6} \ll 1$ and the trajectory can be expanded in orders of $\gamma_0 t^2$:

$$z(t) = z_0 + v_0 t - \frac{1}{2} g_0 t^2 + \gamma_0 t^2 \cdot \left(\frac{z_0}{2} + \frac{v_0 t}{6} - \frac{g_0 t^2}{24}\right) + \mathcal{O}\left(\gamma_0 t^2\right)^2. \tag{2.7}$$

An absolute gravimeter is therefore a simulator for the equation of motion 2.5 that can extract the value of gravity g_0 and, ideally, its gradient γ_0 from the trajectory in equation 2.7.

2.2. Light-pulse interferometry and the mid-point theorem

The idea of using of matter wave interferometers to perform inertial measurements relies on the influence of inertial forces, *e.g.* gravity, on the phase of matter waves. A relevant example is the work by Colella, Overhauser, and Werner on cold neutrons[1] which demonstrated the coupling of the gravitational potential and the phase of matter waves for the first time. The three crystalline silicon gratings constitute beam splitters for the cold neutron waves that manipulate the particles external degrees of

[1] R. Colella et al. *Phys Rev Lett* 34, 1472 (1975) [34]

freedom through a Laue-Bragg diffraction process. Light-pulse atom interferometry realizes functionally identical elements by diffracting atomic matter waves off optical quasi-crystals using Bragg or Raman processes.[2]

[2] J. M. Hogan et al. (2008). arXiv: 0806.3261 [35]

When using dilute clouds, one can neglect inter-atomic interactions and describe the physics of light-pulse atom interferometers at the level of a single atom. The number of atoms in the cloud only, but crucially, matters to mitigate noise sources, most notably quantum projection noise when reading out the interferometric phase. Starting from defined initial internal and external (center of mass) states at the input of the interferometer, a sequence of light pulses creates quantum superpositions of these states that correspond to superpositions of semiclassical trajectories with possibly different internal states. At all times, in particular also between the light pulses, the atomic waves evolve in external potentials, for example of electromagnetic or gravitational nature.

Assuming a pure input state, matter waves can be assigned a unique phase. Interference patterns of matter waves having for example propagated along different semiclassical trajectories are sensitive to the phase difference between the interfering waves. In general, the phase of a pure matter wave depends on its kinematics through the action associated with its center-of-mass trajectory, and interactions with other fields, namely the interferometer's light pulses. In the semiclassical approximation (quantized matter wave, classical optical field), the local phase of the optical field is imprinted on the atomic state upon interaction. When the Hamiltonian describing the matter waves' dynamics between the light pulses is at most quadratic in position and momentum, the differential phase only depends on the center-of-mass position of the interfering matter waves at the times of interaction with the light pulses. This central result is often called "mid-point theorem".[3] It shows that, under most practical conditions, the atom interferometer reduces to a classical experiment where the test object evolves along the mid-point line between the semiclassical trajectories. The final phase then only depends on specific positions along the mid-line trajectory, namely those reached at the times the matter waves interact with the light pulses. Since the optical phase is stored in the matter waves upon interaction, such a light-pulse atom interferometer can be seen as measuring the positions of the matter waves at the times of the light pulses and combining the result into a single scalar phase shift.

[3] C. Antoine et al. *J Opt B - Quantum S O* 5, S199 (2003) [36]

2.3. The Mach-Zehnder-type atomic gravimeter

In 1991, Kasevich and Chu reported a measurement of the gravitational acceleration based on light-pulse atom interferometry.[1] The atom interferometer's geometry they used was analogous to the optical Mach-Zehnder configuration, thus coining the atom interferometer's name. Figure 2.1 shows the associated semiclassical trajectories as well as the corresponding mid-point line. It consists in a series of three temporally equidistant light pulses respectively creating a superposition of the two trajectories ($t = 0$), redirecting them ($t = T$), and recombining them ($t = 2T$) to produce a two-waves interference pattern in the populations of the output ports. The pulses are named $\pi/2$ (beam splitter) and π (mirror) due to the underlying Rabi oscillations between different momentum states and in analogy to the optical Mach-Zehnder setup.

[1] M. A. Kasevich et al. *Phys Rev Lett* 67, 181 (1991) [27]

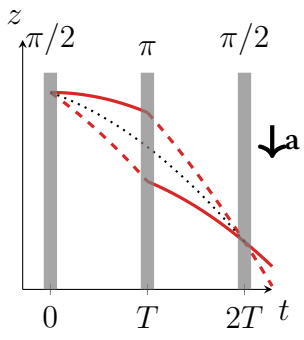

Figure 2.1: Semiclassical geometry of a Mach-Zehnder-like light-pulse atom interferometer. The dotted black curve is the corresponding mid-point line.

In the model of section 2.1, the gravitational potential is given by

$$V(z) = m \int_0^z (g_0 - \gamma_0 \xi)\, \mathrm{d}\xi \tag{2.8}$$

which is quadratic in z. For a diffraction momentum recoil $\hbar k_{\text{eff}}$ and, for simplicity, homogeneous gravity ($\gamma_0 = 0$), the mid-point trajectory reads:

$$z_m(t) = z_0 - \frac{\hbar k_{\text{eff}}}{2m} t - \frac{1}{2} g t^2 \tag{2.9}$$

where z_0 is the center-of-mass position of the input state upon entering the interferometer. A direct application of the mid-point theorem gives the interferometric phase: [36, eq. 16]

$$\begin{aligned} \Delta\phi &= +k_{\text{eff}} z_m(0) + (-k_{\text{eff}} - k_{\text{eff}}) z_m(T) + (-(-k_{\text{eff}})) z_m(2T) \\ &= k_{\text{eff}} \left[z_m(0) - 2 z_m(T) + z_m(2T) \right] && (2.10) \\ &= -k_{\text{eff}} g T^2. && (2.11) \end{aligned}$$

[2] A. Peters et al. *Metrologia* 28, 25 (2001) [28]

By extension, the interferometric phase in the case $\gamma_0 \neq 0$ reads:[2]

$$\Delta\phi = (k_{\text{eff}}T^2)g_0 + (k_{\text{eff}}T^2)\gamma_0 \cdot \left[\frac{7}{12} g_0 T^2 - \underbrace{\left(v_0 + \frac{\hbar k_{\text{eff}}}{2m} \right)}_{\bar{v}_0} T - z_0 \right] + \mathcal{O}\left(\gamma_0 T^2\right)^2 . \tag{2.12}$$

The quantity $\bar{v}_0$ is the velocity of the mid-point trajectory and stems from the application of the mid-point theorem.

Equation 2.10 is generic and is valid as long as the mid-point theorem holds. It supports the interpretation of the mid-point theorem discussed in section 2.2: the interferometric phase is an algebraic combination of the mid-point positions at the atom-light interaction times, scaled by $k_{\text{eff}} \sim 1/\lambda$, the position measurement resolution. When $\gamma_0 = 0$, the mid-point trajectory is parabolic (eq. 2.9) and three measurements determine it completely. This is not the case anymore when $\gamma_0 \neq 0$. Then, the bracketed quantity in equation 2.10 is a centered finite difference approximation of the trajectory's second derivative at $t = T$.[3] Assuming that the trajectory is four times continuously differentiable, the exact finite difference formula reads:

[3] A. M. Nobili et al. *Phys Rev Research* 2, 012036 (2020) [37]

$$\frac{\mathrm{d}}{\mathrm{d}z}(\Delta t) = \frac{1}{T^2}\left(z_m(0) - 2z_m(T) + z_m(2T)\right) - \frac{1}{12}T^2\frac{\mathrm{d}^4}{\mathrm{d}t^4}z_m(\xi) \tag{2.13}$$

where $0 \leq \xi \leq 2T$.[4] Replacing the mid-point trajectory by the model in equation 2.7, the fourth-derivative of the position is time-independent ($z_m^{(4)}(t) = -g_0\gamma_0$) and the difference between $\ddot{z}_m(T)$ and $\Delta\Phi/(k_{\text{eff}}T^2)$ from equation 2.12 is indeed the quantity predicted by the finite difference residuals. This confirms that, when the mid-point theorem applies, the Mach-Zehnder-like light-pulse atom interferometer realizes a centered finite difference approximation of the mid-point trajectory's second derivative (acceleration) at $t = T$. In the presence of a gravity gradient, the inferred value of gravity does not necessarily equal the real value in the middle of the interferometer ($z_m(T)$), despite the apparent temporal symmetry.

[4] J. Rappaz et al. Presses polytechniques et universitaires romandes, 2010 [38]

It is relevant to generalize the approach presented here to higher orders. Very early,[5] multi-loop interferometers, such as for example the $\pi/2 - \pi - \pi - \pi/2$ geometry, have been proposed to access higher-order derivatives of the gravity field. Here, the differences between the laser-interferometric falling corner

[5] J. F. Clauser. *Physica B* 151, 262 (1988) [39]

cube sensors and the light-pulse matter wave interferometers are stringent. In the first case, the expected trajectory, often according to the model of equation 2.7, is adjusted to the individual samples of the test masses' trajectory with a least-squares method. The typically hundreds of samples then allow determining the low orders of the gravity field.[6] On the contrary, light-pulse atom interferometers do not provide access to the individual measurements but aggregate them, summing the circulation of the matter waves' phases on the interferometer's different loops.[7] Each Mach-Zehnder-like loop has a contribution of the form $z_{n-1} - 2z_n + z_{n+1}$ where z_n is a shorthand for $z_m(nT)$. Two consecutive loops with pulses at times $t = -2T$ ($\pi/2$), $t = -T$ (π), $t = T$ (π), and $t = 2T$ ($\pi/2$) therefore have a contribution:

[6] T. M. Niebauer et al. *Metrologia* 48, 154 (2011) [40]

[7] P. Storey et al. *J Phys II France* 4, 1999 (1994) [41]

$$\begin{aligned}\Delta\phi \propto \frac{1}{T^3}\left[(z_2 - 2z_1 + z_0) - (z_0 - 2z_{-1} + z_{-2})\right] \\ = \frac{1}{T^3}\left[z_2 - 2z_1 + 2z_{-1} - z_{-2}\right]\end{aligned} \quad (2.14)$$

which is a centered finite difference formula for the third derivative of the position at $t = 0$. The truncation error scales again with T^2. Contrary to differential schemes, such multi-loop geometries are inherently insensitive to lower-order signals. Nevertheless, using appropriate methods to reject spurious interferometers, they offer competitive sensitivities for inertial sensing[8,9] and illustrate the versatility of atom interferometry where purpose-tailored geometries can easily be programmed, without changing the hardware.

[8] C. Schubert et al. (2021). arXiv: 2102.00991 [42]

[9] L. A. Sidorenkov et al. *Phys Rev Lett* 125, 213201 (2020) [43]

2.4. Limiting noise considerations

Compared to optical interferometers, light-pulse atom interferometers swap the roles of light and matter. In optical interferometers, the light constitutes the phase memory and is manipulated by material elements (mirrors, beam splitters). Conversely, in light-pulse atom interferometers the matter waves hold the interferometric phase, and are diffracted by light gratings. This has a direct consequence on the operation of a metrological instrument based on such technologies. For optical interferometers, lasers can behave as continuous coherent light sources. The matter wave equivalent is the atom laser, a long standing quest in the field of atom optics with applications also in frequency metrology.[1] While metrologically usable

[1] W. Ketterle. *Rev Mod Phys* 74, 1131 (2002) [44]

devices now become available, their realization is still extremely complex.[2] On the other hand, pulsed sources have reached very high-performance as well as compactness and ruggedness,[3] making them more promising candidates for near-future atom-interferometry-based metrology.

Light-pulse atom interferometers are therefore typically sampling devices whose measurement cycle starts with the preparation of the atomic sample, followed by the realization of the interferometric sequence, and ends with the readout of the interferometric phase. Outside of the interferometric sequence, the instrument is insensitive to the quantity of interest, thus leading to an aliasing effect similar to the Dick effect experienced by atomic clocks.[4] This aliasing is strongly reduced when interleaving the interferometric sequences, thus effectively nulling the dead time between cycles,[5] but still present due to the fact that the interferometer aggregates the acceleration information during one interferometric sequence into a single phase shift.

The detection of the interferometric phase contains another key noise source. Similarly to optical interferometers, the phase is read out by comparing the intensities in the interferometer's output ports. For matter wave interferometers, this corresponds to counting the number of atoms (intensity) in a given state (output port) through a quantum-mechanical projective measurement. For independent particles, the detection noise is bounded from below by $1/\sqrt{N}$ where N is the total number of particles (Poisson statistics). Using correlated ensembles gives the perspective of a lower bound scaling with $1/N$.[6] This provides the motivation for using large atomic ensembles, thus lowering this shot-noise limit even when using uncorrelated atomic samples.

Quantitatively, the response of the interferometer to infinitesimal phase changes is described by its temporal sensitivity function $g(\tau)$.[7] By integration, the sensitivity function corresponds to the weighting of phase variations (spurious or wanted, e.g. from the light pulses) in the final interferometric phase. Its Fourier transform is therefore linked to the instrument's complex transfer function $H(\omega)$. One can show that the interferometric phase's Allan variance scales as: [49, eq. 16]

$$\sigma_\phi^2(\tau) = \frac{1}{\tau}\sum_{n=1}^{\infty}\left|H\left(\frac{2\pi n}{T_c}\right)\right|^2 S_\phi\left(\frac{2\pi n}{T_c}\right) \tag{2.15}$$

where τ is the integration time, S_ϕ the phase-noise power spectral density and $T_c = T_p + 2T$ the total cycle time (T_p is the sample preparation time). The sampling of phase noise at multiples of

[2] C.-C. Chen et al. *Phys Rev Applied* 12, 044014 (2019) [45]

[3] J. Rudolph et al. *New J Phys* 17, 065001 (2015) [46]

[4] G. J. Dick. 1987 [47]

[5] D. Savoie et al. *Sci Adv* 4, eaau7948 (2018) [48]

[6] F. Anders et al. (2020). arXiv: 2010.15796 [10]

[7] P. Cheinet et al. *IEEE T Instrum Meas* 57, 1141 (2008) [49]

the cycle frequency corresponds to the aliasing effect anticipated before. Since acceleration is linked to phase through the scale factor $k_{\text{eff}}T^2$ (equation 2.11), we can express this Allan variance in terms of the acceleration power spectral density: [49, eq. 19]

$$\sigma_\phi^2(\tau) = \frac{k_{\text{eff}}^2}{\tau} \sum_{n=1}^{\infty} \frac{|H(2\pi n/T_c)|^2}{(2\pi n/T_c)^4} S_a\left(2\pi n/T_c\right). \tag{2.16}$$

The shot-noise-limited noise level can be evaluated by applying equation 2.15 for white phase noise. One finds: [49, eq. 17]

$$\sigma_\phi^2(\tau) \propto S_\phi \frac{T_c}{\tau} \propto \frac{T_c}{N\tau} \tag{2.17}$$

where we substituted $S_\phi = 1/N$ to obtain the shot-noise limit. This finally leads to an estimator for an atomic gravimeter's short-term (in the white phase noise regime), shot-noise limited stability:

$$\sigma_a(\tau) \sim \frac{\sqrt{T_p + 2T}}{\sqrt{N} k_{\text{eff}} T^2} \frac{1}{\sqrt{\tau}}. \tag{2.18}$$

This expression is the motivation for striving towards fast creation of large atomic ensembles in light-pulse atom interferometers. Not only does the short preparation time mitigate the aliasing effect and enables better interleaved operation strategies, but the large number of atoms also pushes down the shot-noise limit. For the Hannover VLBAI facility, we developed a novel, robust, and high-flux source of cold ytterbium atoms[8] as a first step towards effective atom interferometry with ytterbium atoms. The motivation for ytterbium is given in chapter 5 where we discuss tests of the universality of free fall and quantum clocks.

[8] E. Wodey et al. *J Phys B: At Mol Opt Phys* 54, 035301 (2021) [50]

3. Specific challenges in very long baseline atomic absolute gravimetry

An interferometer's phase shift typically scales with the enclosed area. For the optical Mach-Zehnder geometry, this is the spatial area between the arms. For the light-pulse variant from section 2.3, it is the area defined by the inverse of the recoil momentum ($1/k_{\text{eff}} \sim \lambda_{\text{eff}}$) and the total travel distance, which is proportional to the pulse separation time T squared. This is for example visible in the phase shift formula displayed in equation 2.11. This scaling fits our interpretation in terms of subsequent position measurements. The overall sensitivity must scale with the ratio of the distance measured ($\propto T^2$) to the measurement resolution (λ_{eff}). Increasing the *scale factor* $k_{\text{eff}}T^2$ is therefore the primary handle (next to noise mitigation) to increase an atomic gravimeter's stability.

There are two ways of increasing the scale factor: on the one hand, the recoil momentum can be increased by the use of large momentum transfer (LMT) beam splitters relying on high diffraction orders,[1] Bloch oscillations,[2] or combinations thereof.[3] On the other hand, the pulse separation time can be scaled up, with a quadratic dependency. This is one of the main drivers for microgravity operation where the vacuum chamber is falling at the same rate as the matter waves.[4] On the ground, folding the free fall path in fountain geometries also provide larger pulse separation times. A more straightforward, and complementary approach, is to simply extend the baseline length, as pursued in this work.

Very long baseline atom interferometry (VLBAI) represents the class of instruments with vertical baselines in the 10 m range and above. Compared to typical lab-scale or transportable instruments, the 50-fold increase in baseline length translates into a 50-fold gain in the scale factor. Applying equation 2.18

[1] H. Müller et al. *Phys Rev Lett* 100, 180405 (2008) [9]

[2] P. Cladé et al. *Phys Rev Lett* 102, 240402 (2009) [51]

[3] H. Müller et al. *Phys Rev Lett* 102, 240403 (2009) [52]

[4] H. Müntinga et al. *Phys Rev Lett* 110, 093602 (2013) [53]

with a preparation time $T_p = 3\,\mathrm{s}$, $N = 10^6$ atoms, and first-order diffraction $k_{\mathrm{eff}} = 4\pi/(780\,\mathrm{nm})$, one gets the following shot-noise-limited instabilities:

$$\sigma_a(1\,\mathrm{s}) = \begin{cases} 800\,\mathrm{pm/s^2} & \text{for } T = 400\,\mathrm{ms} \text{ (drop)} \\ 100\,\mathrm{pm/s^2} & \text{for } T = 1.2\,\mathrm{s} \text{ (launch).} \end{cases} \tag{3.1}$$

These short-term instabilities are only a factor 10 higher than the typical performance of superconducting gravimeters. In addition, the VLBAI gravimeter has high extension capability. For example, using larger momentum transfer beam splitters could fill the gap to, or even outperform, superconducting instruments. Also, a VLBAI gravimeter would be absolute, thus removing the need for the periodic (small) drift calibration carried out for superconducting devices.

At a technically high level, the challenges for VLBAI gravimetry are two fold, mirroring the two defining quests of metrology. First, enable shot-noise limited operation with a large number of atoms such that the measurement instability reaches the levels of equation 3.1 and better. Second, constrain the systematics at this level, thus realizing a new gravimetry standard. Paths towards these goals are also split between two main branches. On the one hand, control over the atom-optics processes must be achieved to enable shot-noise limited operation. Here, the novelty of the extended baseline is linked to the long evolution times and key techniques are shared with those developed for microgravity instruments, like for example matter wave lensing to reduce the wave packet expansion.[5,6] On the other hand, the accuracy for ground-based absolute measurements is limited both by instrument-internal imperfections (e.g. wavefront distortions) and coupling to the environment.

[5] D. Becker et al. *Nature* 562, 391 (2018) [54]

[6] T. Kovachy et al. *Phys Rev Lett* 114, 143004 (2015) [55]

In this chapter, we review two such effects, which limit the stability and accuracy of a VLBAI gravimeter and are amplified by the use of a very long baseline for absolute instruments. First, due to the equivalence principle, sensitivity to motion of the inertial reference is magnified by the same scale factor as the sensitivity to accelerations of the matter waves' center of mass. This creates serious challenges on the inertial reference's vibration control which we outline in section 3.1, together with the strategies envisaged for the Hannover VLBAI facility. Second, the instrument's large spatial extent leads to significant gravity variations along the baseline. The dominant effect is the free-air gradient γ_0 (equation 2.4), modified by the local environment. The presence of large building structures, like for example the

floors the device spans across, introduces anharmonicities in the gravitational potential (curvature in the acceleration field) that imply a departure from the hypotheses of the mid-point theorem. In section 3.2, we build on our work modeling and mapping the gravitational acceleration along the instrument's baseline[7] to estimate the systematic effect of acceleration curvature on a VLBAI gravimeter.

In chapter 5, we present other research directions where the extended size of the baseline fundamentally matters for the realization of the experiment (e.g. macroscopically de-localized quantum superposition states). For absolute gravimetry however, the extended baseline is only the conceptually simplest idea that enables larger free fall times and therefore higher scale factors. The effects discussed in this chapter, as well as the engineering effort described in chapter 4, show nevertheless that more compact sensing concepts keeping the large interferometric area would provide easier control of stray fields and the associated systematics. A promising idea would therefore be to bound the extent of the matter waves' semiclassical trajectories while keeping long interferometric times. Driven by the quest for highly sensitive transportable sensors, approaches for example suspending the matter waves in optical standing waves have been proposed[8] and realized.[9] This method parallels the operation principle of a superconducting gravimeter, but nevertheless provides an absolute measurement since the levitation force that locally counteracts gravity is linked to an absolute frequency measurement. A major limitation for this concept is linked to the extended time spent by the atoms interacting with the noisy light field. Recently, a major milestone was achieved with the demonstration of 20 s phase-coherent holding time using an optical cavity to reduce waveform distortions.[10] Alternatively, juggling with the atomic test masses allows reducing the total interaction time with the light, while keeping the small sensing volume.[11,12] The control of systematics associated to the holding or relaunching field's light shifts nevertheless remains a major obstacle for reaching very high accuracies with these sensing geometries, and an active field of research.

[7] M. Schilling et al. *J Geodesy* 94, 122 (2020) [56]

[8] P. Cladé et al. *Europhys Lett* 71, 730 (2005) [57]

[9] R. Charrière et al. *Phys Rev A* 85, 013639 (2012) [58]

[10] V. Xu et al. *Science* 366, 745 (2019) [59]

[11] S. Abend et al. *Phys Rev Lett* 117, 203003 (2016) [60]

[12] M. Andia et al. *Phys Rev A* 88, 031605 (2013) [61]

3.1. Inertial reference seismic isolation

In section 2.3, we showed that, under the assumptions of the mid-point theorem, a Mach-Zehnder-like atomic gravimeter is equivalent to measuring the position of a test mass at three different moments during its free fall and forming a centered finite difference expression from these points. This notably assumes

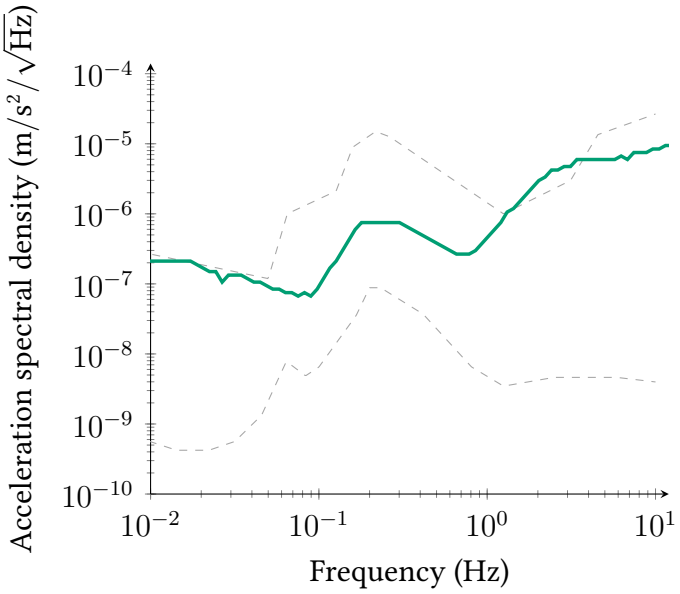

Figure 3.1: Seismic noise recorded at the Hannover VLBAI site. The presented data is the recorded probabilistic power spectral density's square root mode. The dashed lines represent the Peterson new high and low noise models [63].

the presence of a reference system to which the measurements are anchored. Put differently, one needs to define, and realize experimentally, the inertial frame in which the acceleration of the test mass is measured. In light-pulse atomic gravimeters, the inertial frame is typically realized by a mirror that retro-reflects the light pulses in order to obtain the diffraction quasi-crystals. The optical equiphase fronts, spatially separated by $\sim 1/k_{\text{eff}}$, are therefore referenced to the zero on the mirror's surface which constitutes the measurement's reference frame.

When operated at their shot-noise limit, atomic gravimeters improve their stability when increasing their scale factor $k_{\text{eff}}T^2$. Imperfections of the inertial reference due to seismic noise is however limiting the short-term stability of the most advanced devices, as hinted to by their use of different pulse separation times T to achieve very similar performance.[1,2,3] Vibration control is therefore a key element to be able to exploit VLBAI gravimeters to their full potential.

Figure 3.1 shows the background seismic activity measured at the Hannover VLBAI facility site. The Peterson new high noise (NHNM) and low noise (NLNM) models[4] are displayed for reference. They describe the typical limits for natural seismic activity. Excursions above the high noise model in the few hertz range originate from the location of the hosting building in the middle of the city of Hannover, with neighboring automobile and tramway traffic. Using equation 2.16, we calculate the

[1] Z.-K. Hu et al. *Phys Rev A* 88, 043610 (2013) [62]

[2] C. Freier et al. *J Phys: Conf Ser* 723, 012050 (2016) [29]

[3] P. Gillot et al. *Metrologia* 51, L15 (2014) [7]

[4] J. Peterson. *U.S. Geological Survey open-file report* 93, 322 (1993) [63]

vibration-limited instability of an atomic gravimeter operated with 10^6 atoms prepared in $T_p = 3$ s and first-order diffraction. The result is shown as a function of the pulse separation time T in figure 3.3 (dark blue curve). At $T \approx 400$ ms, corresponding to a simple drop using the full baseline length (see chapter 4), the vibration-limited instability is 1×10^{-6} m/s^2 at 1 s, three orders of magnitude away from the corresponding shot-noise limit. The general behavior of the interferometer's stability versus pulse separation time T is the combination of the low-pass behavior of the interferometer's transfer function[5] with a corner around $1/(2T)$ and a scaling due to the scale factor variation.

Two complementary approaches can be pursued to improve on this situation. First, vibration isolators can offer multiple tens of decibels of attenuation above their resonance frequency. For the Hannover VLBAI facility, we foresaw a geometric anti-spring (GAS) -based seismic attenuation system (SAS) that builds on the developments made for optical gravitational wave detectors.[6] Figure 3.2 is a photograph of the commercial system[7] featuring a fundamental (vertical mode) resonance frequency of 320 mHz. Modeling the isolation platform, one gets its displacement transfer function and therefore its vibration attenuation behavior. Applying the measured seismic activity as input and assuming critical damping of the isolator's resonance,[8] one obtains the light blue curve in figure 3.3 for the vibration-limited instability. The effect of damping is two-fold: on the one hand, it flattens the isolator's gain around the resonance frequency, which avoids adding unwanted noise in the interferometer's sensitive frequency band. On the other hand, it decreases the isolation roll-off at higher frequency, transitioning from a $1/f^2$ to a $1/f$ damping, thus increasing the impact of higher frequency noise.

The second key approach to decreasing the impact of seismic noise is correlation with an auxiliary sensor. Knowing the interferometer's sensitivity function (section 2.4), one can calculate the effect of an instantaneous event on the interferometric phase and therefore correct for it either *in situ*, for example as a counteracting phase jump on the last light pulse,[9] or *a posteriori*, by applying the phase correction upon data evaluation. Such techniques are in particular key to the operation of commercial gravimeters[10] without vibration isolation, thus increasing their transportability and ease of deployment. This hybridization may be seen in analogy to atomic clocks, where a good short term reference (the local oscillator, here the auxiliary motion sensor) is corrected by an atomic reference at the longer timescales. The Hannover VLBAI SAS platform is equipped with a high-performance triaxial seismometer[11] to

[5] P. Cheinet et al. *IEEE T Instrum Meas* 57, 1141 (2008) [49]

[6] M. G. Beker et al. 2012 [64]

[7] Innoseis BV, Amsterdam, The Netherlands

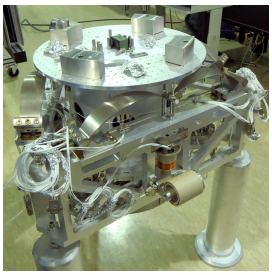

Figure 3.2: Photograph of the GAS-based seismic attenuation system for the Hannover VLBAI facility.

[8] G. Bergmann. PhD thesis. Leibniz Universität Hannover, 2018 [65]

[9] J. Lautier et al. *Appl Phys Lett* 105, 144102 (2014) [20]

[10] V. Ménoret et al. *Sci Rep* 8, 1 (2018) [66]

[11] Nanometrics Trillium T240VP

track the movement of the interferometer's inertial reference. Assuming perfect correlation with such a sensor operating at its best noise performance, vibration noise is not limiting to reach the shot noise level in simple drop operation (red curve in figure 3.3). Going in the direction $T \gtrsim 1$ s however, the red-filled area shows the need for even better sensors.

The performance projection assuming perfect tracking with the Nanometrics Trillium 240 sensor is however pretty optimistic. Because such high-performance sensors are designed for Earth observation and exploration, their reference plane is on the bottom of the housing and they cannot be mounted upside-down. Positioning the inertial reference on top of the apparatus is problematic due to the mounting of the vibration isolator and the low-frequency oscillations of the tower (see section 4.1). Commercial, off-the-shelf sensors are also usually not compatible with in-vacuum operation, a necessary condition to reduce acoustic coupling on the isolated platform. Similarly to the design of the LIGO gravitational wave detector, the commercial devices mounted on the VLBAI SAS are placed in anti-vacuum pods to isolate them from the vacuum outside.

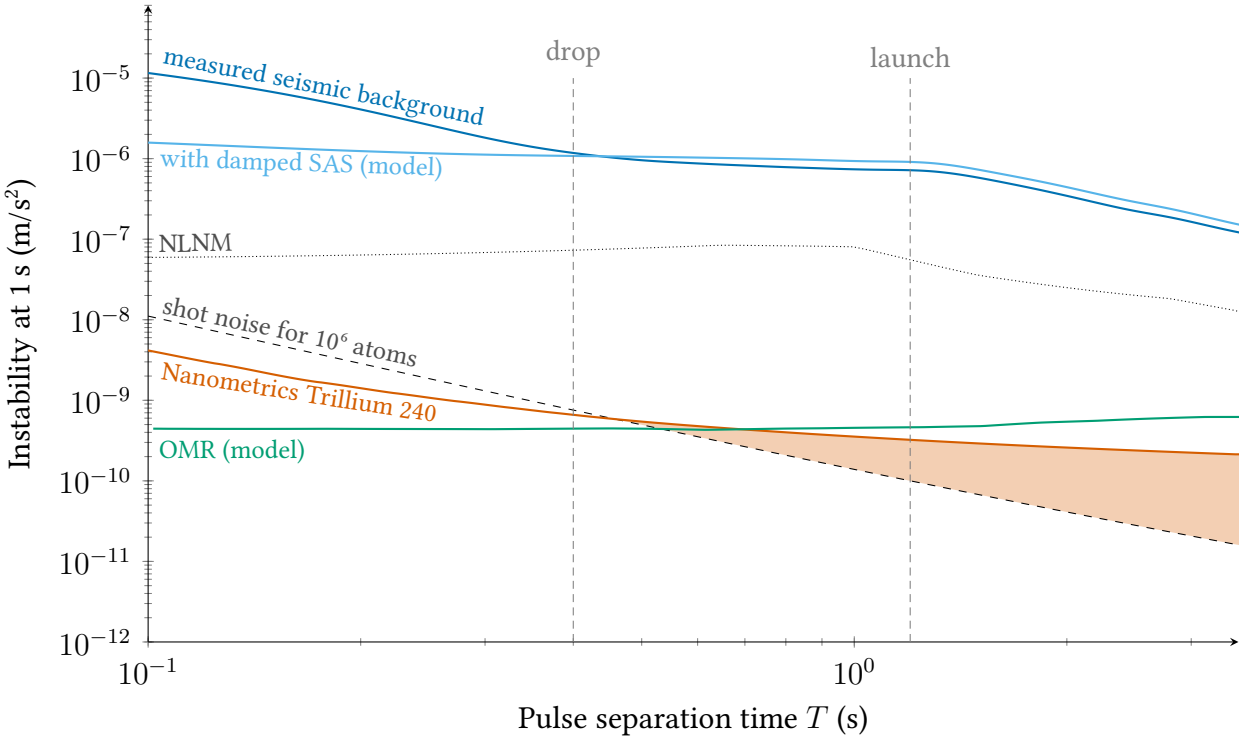

Figure 3.3: Projected short-term instability of VLBAI gravimeter geometries depending on the level of seismic noise control. For the auxiliary sensors, we assume ideal noise tracking down to their best tabulated performance. Like for all other projections in this manuscript, we assume $N = 10^6$ atoms, a sample preparation time $T_p = 3$ s, and first order diffraction.

Miniature opto-mechanical resonators[12] (OMR) have large potential for high-performance inertial sensing with atom interferometry. Their small size and glass substrate make their integration with the retro-reflection mirror easy. Novel designs may even use the mirror itself as part of the optical sensing cavity.[13] Also, their optical readout avoids electrical noise feed-through and simplifies their operation in a vacuum environment. Finally, the control over their manufacturing process allows tuning their operating parameters (quality factor/finesse and resonance frequency) to the application, making such motion sensors very versatile. This is particularly relevant in the context of VLBAI gravimetry as one can engineer the resonance frequency and quality factor to take fully advantage of the SAS's suppression factor at high frequencies.

[12] O. Gerberding et al. *Metrologia* 52, 654 (2015) [67]

[13] L. L. Richardson et al. *Appl Optics* 59, G160 (2020) [68]

As pathfinder for the development of the VLBAI inertial reference, we demonstrated the first correlation of a motion-sensing opto-mechanical resonator with an atom interferometer.[14] The advanced sensor discussed in figure 4 of reference [69] already enables shot-noise-limited operation in the simple drop mode (green curve in figure 3.3). Further development of such sensors, for example towards lower resonance frequencies, thus increasing the low-frequency sensitivity, will allow reaching the shot-noise in launch configurations. In addition, the small physical footprint and all-optical readout capability of these sensors make them ideal candidates for better monitoring of the SAS's platform without introducing spurious noise through undesired electrical loops. Finally, interleaved operation will reduce noise aliasing by suppressing inter-cycle dead time, as already demonstrated for gyroscopes.[15]

[14] L. L. Richardson et al. *Commun Phys* 3, 208 (2020) [69]

[15] D. Savoie et al. *Sci Adv* 4, eaau7948 (2018) [48]

3.2. Gravity profile along the baseline

The large physical extent of a VLBAI apparatus naturally opens the possibility of increased field variations along the interferometer's baseline compared to transportable instruments. While local gradients may be higher in the latter type (due to the required compactness, all necessary equipment needs to be located close to the baseline),[1] the overall variation is likely larger on VLBAIs. External fields contradict, to a variable extent, the free fall hypothesis for the atomic test masses. The interactions of the atomic matter waves with external fields are very well understood and their magnitudes generally scale with the gradient of the external field. However, correcting the associated systematic effect to a level not limiting the instrument's accuracy requires a precise knowledge of the field. The general strategy is to control

[1] N. Heine et al. *Eur Phys J D* 74, 174 (2020) [33]

and shield the external fields. As described in sections 4.3 and 4.4, this provides an electromagnetic environment that is only limiting at the few pm/s^2 level, a sensitivity grade only achieved with extended time interferometers transferring above 100 recoils per beam splitter. Fundamentally, effective shielding smooths the external fields such that the field curvature is negligible and therefore the hypotheses of the mid-point theorem apply.

The observations in the last paragraph do not apply to gravity variations. First, by definition, the test masses are in free fall even if gravity is not homogeneous. This poses the question of the instrument's effective height: what does the one value of gravity linked to the interferometric phase correspond to when gravity is not constant along the baseline? Second, the presence of gravity curvature (and higher orders) makes the associated potential cubic (or more) and therefore depart from the validity conditions of the mid-point theorem. Both points lead to systematic effects that need to be taken into account when evaluating a VLBAI gravimeter's accuracy.

We motivated the use of very long baselines for precision gravimetry using the scale factor $k_{\text{eff}}T^2$ between the local acceleration and the interferometric phase in equation 2.11. However, when considering the finite difference formula realized by the Mach-Zehnder-type atom interferometer (equation 2.13), increasing the pulse separation time makes little sense, as it quadratically increases the corresponding truncation error.[2] The free-air gradient (–3.1 µm/s^2/m, equation 2.4) indeed couples position uncertainties of 1 mm to gravity value uncertainties of 3 nm/s^2. The effect on the instrument's effective height must therefore be constrained to the sub-mm level. We give an analytical treatment of the effective height issue in the case of a pure gravity gradient in our article.[3]

The more fundamental issue is linked to the appearance of cubic and higher-order terms in the gravitational potential. This invalidates in principle the mid-point theorem and, in extreme cases, the interferometric phase can fully decouple from the underlying trajectory.[4] In more moderate cases, perturbation theory can be used to evaluate the effect, as was already done for the self-attraction of a transportable instrument.[5] Figure 3.4 shows the individual components of the model derived in our article (ref. [56]). The full model is composed of a reference gravity value $g(z = 0)$, the free-air gradient $\gamma_0 = 3.1\,\mu\text{m/s}^2/\text{m}$ (equation 2.4), and corrections due to the local ground density (Δg_g) and the building's attraction (Δg_b). We linearize all those contributions and gather the non-linear parts in a single perturbation term δg. The model therefore reads:

[2] A. M. Nobili et al. *Phys Rev Research* 2, 012036 (2020) [37]

[3] M. Schilling et al. *J Geodesy* 94, 122 (2020) [56]

[4] C. Overstreet et al. *Am J Phys* 89, 324 (2021) [70]

[5] G. D'Agostino et al. *Metrologia* 48, 299 (2011) [71]

$$g(z) = (g_0 + \Delta g_{g,0} + \Delta g_{b,0}) - (\gamma_0 + \gamma_g + \gamma_b)\, z + \delta g(z) \qquad (3.2)$$

where $\Delta g_{g,0} = -7\,\mathrm{nm/s^2}$ and $\gamma_g = -219\,\mathrm{nm/s^2/m}$ are the constant and linear parts of the ground correction, and $\Delta g_{b,0} = -727\,\mathrm{nm/s^2}$ and $\gamma_b = -126\,\mathrm{nm/s^2/m}$ linearize the building's attraction. The resulting gradient is $\gamma = -2.741\,\mu\mathrm{m/s^2/m}$. Despite an amplitude of $213\,\mathrm{nm/s^2/m}$, the residuals (right panel in figure 3.4) are small enough to fulfill the perturbation theory conditions.[6] The bias acceleration on the reference interferometer described in chapter 4 and spanning the pink region in figure 3.4) is $-23\,\mathrm{nm/s^2}$. The uncertainty on the model used for this calculation is $20\,\mathrm{nm/s^2}$ and thus limits the accuracy of the bias correction to that level. Further refinements to the model are expected to bring its accuracy in the sub $10\,\mathrm{nm/s^2}$ domain [56].

[6] C. Ufrecht et al. *Phys Rev A* 101, 053615 (2020) [72]

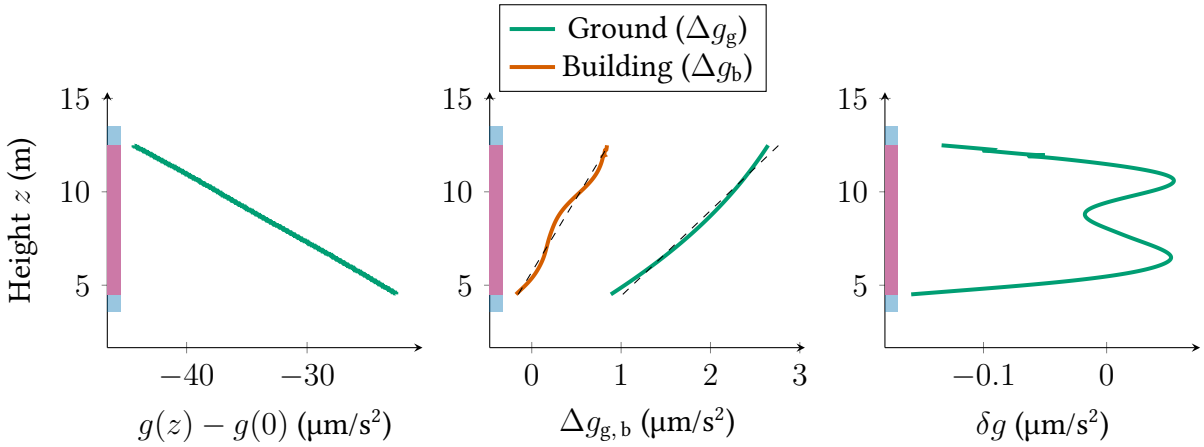

Figure 3.4: Gravity model along the Hannover VLBAI facility's baseline. **Left**: full model, dominated by the free air gradient. **Middle**: ground (Δg_g) and building attraction (Δg_b) contributions, with associated linear adjustments. **Right**: non-linear residuals on the full model resulting from the linear approximation in the middle panel. The blue and pink areas mark the extent of the magnetic shielding and *region of interest* for precision interferometry respectively (see chapter 4). Data from reference [56].

Also, a full assessment of the effect of gravity gradients on the Hannover VLBAI facility requires extensions to the gravity model. In particular, the structures forming the baseline hardware (see chapter 4) are not yet included. The work presented in reference [56] is nevertheless the necessary solid foundation for such extensions, as it allows to validate the model against a reference profile [56, §6].

Beyond the mostly static part considered here, dynamic effects

affect the local value of gravity. Global effects like e.g. tides are well modeled and their impact is practically the same on all points along the baseline. On the contrary, as discussed in reference [56], local effects like e.g. groundwater level variations can have different impacts on local gravity versus height due to the structure of the building's foundations. This creates additional curvature in the gravity field whose impact we estimate at the $5\,\mathrm{nm/s^2}$ level.

4. Baseline design and characterization

In this chapter, we discuss in more details the realization of the Hannover VLBAI facility's baseline. Figure 4.1 shows an overview of the apparatus, based on a digital model. It consists of three main components: upper and lower ultracold atoms sources (in green), the inertial reference with, in particular, the in-vacuum geometric anti-spring-based seismic attenuation system discussed in section 3.1 (in orange), and the central element, the magnetically shielded baseline (in blue). In this chapter, we describe this latter component and present some associated characterization measurements and their physical consequences.

Strictly speaking, the baseline is the geodesic along which the atoms fall while undergoing the atom-interferometric sequence, ideally only disturbed by the well-controlled light pulses. By extension, we call *baseline* the hardware installed to provide the quiet and homogeneous environment required for high-precision atom interferometry and depicted in figure 4.2: a ultra-high vacuum chamber (section 4.2) with high-performance magnetic field control (section 4.3) and precise temperature monitoring (section 4.4). These components are physically constrained in the building by a highly stable mechanical construction described in section 4.1.

For each sub-component, we describe the physics underlying the associated systematic effects, derive the corresponding engineering requirements, present their implementation, and finally evaluate their efficiency given the available characterization data. For the latter step, we evaluate the perturbing effect only inside the *region of interest* for high-precision atom interferometry where the magnetic gradients are the smallest, defined to span the inner 8 m of the shielded volume, *i.e.* heights 4.5 m to 12.5 m (marked in pink in figure 4.1). More precisely, we define a *reference interferometer*

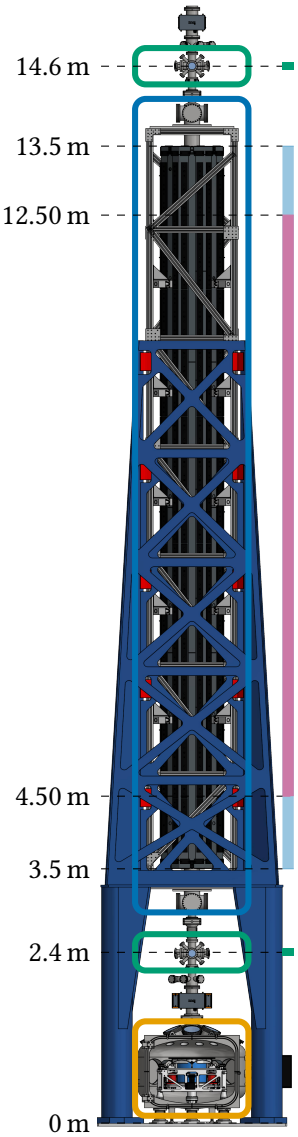

Figure 4.1: Overview of the Hannover VLBAI apparatus (false colors).

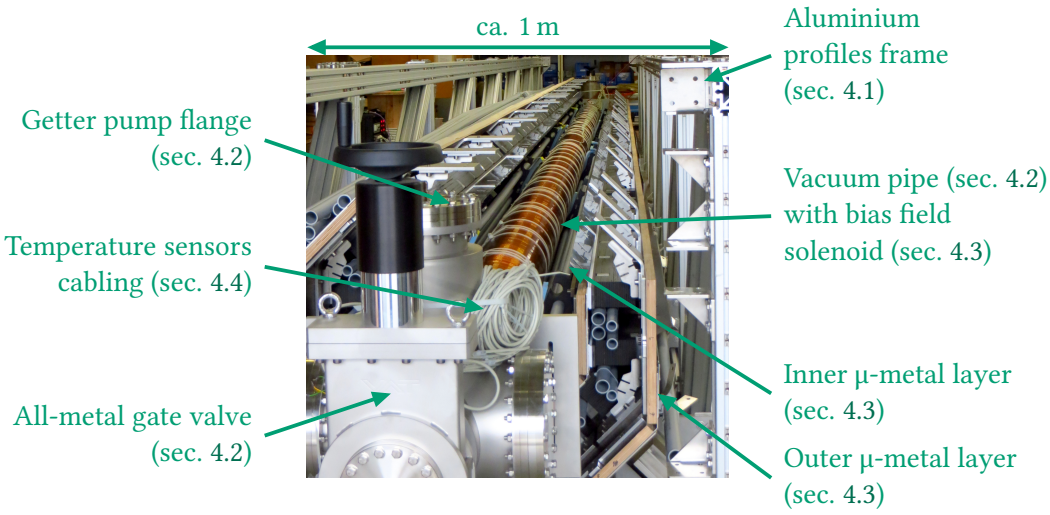

Figure 4.2: Longitudinal view of the assembled baseline for the Hannover VLBAI apparatus. One quarter of both shield layers are removed to allow inserting the vacuum system.

that is the simplest full-baseline drop geometry. The region of interest is 8 m long. However, it starts 2 m below the top chamber, such that, if released with zero velocity, the matter waves' center of mass fall with more than 6 m/s upon entering the interferometer, which limits the pulse separation time T. The reference interferometer has the following parameters:

Pulse separation time T: 385 ms
Total free fall time: 660 ms $+ 2T +$ 150 ms (detection in the lower atomic source chamber)
Velocity at first $\pi/2$ **pulse:** 6.5 m/s
Atomic species: ^{87}Rb
Recoil per pulse: $4\pi/780$ nm.

The mid-point trajectories are calculated using equation 2.7 in the linear truncation of the device's gravity model[1] (section 3.2). We then apply perturbation theory[2] to calculate the magnitude of the systematic effect under consideration on the reference interferometer. This gives an upper bound to the magnitude of the corresponding bias. When projecting a VLBAI gravimeter's accuracy budget, we assume that the bias uncertainty will be known at least to this level.

[1] M. Schilling et al. *J Geodesy* 94, 122 (2020) [56]

[2] C. Ufrecht et al. *Phys Rev A* 101, 053615 (2020) [72]

4.1. Mechanical construction

The apparatus depicted in figure 4.1 has a total weight of approximately 16 000 kg. In particular, the magnetically shielded baseline weighs around 7500 kg and needs to span the space

between 3.5 m and 13.5 m above the building's foundation. This section describes the *support structure* holding the baseline hardware and the upper atomic source at their target positions. Beyond the requirements on its mechanical stability, the support structure must also have a low and homogeneous magnetic susceptibility, in order not to produce strong magnetic field inhomogeneities in the direct vicinity of the baseline's magnetic shield.

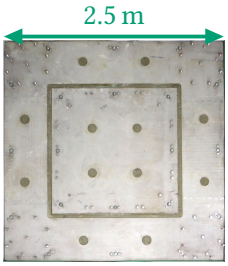

Figure 4.3: Top view of the freshly installed and potted base plates.

At the bottom of the instrument, a set of two 3 cm thick, stainless-steel, concentric base plates provides the solid ground to hold the full instrument. A point on their upper surface also defines the vertical origin for all geodetic measurements (and therefore the height coordinates in figure 4.1). Figure 4.3 shows the base plates just after their installation in the building. The inner square supports only the sensitive inertial reference platform, its vacuum enclosure, and the lower atomic source, for a total of around 1500 kg. The outer one constrains the spacing of the support structure's feet and therefore supports the weight of the rest of the instrument (around 14 500 kg). The base plates rest on ca. 5 cm high adjustable feet which allow to compensate for the unevenness of the building's raw foundation just beneath them. After leveling, we fastened the inner and outer base plates into the building's foundation with respectively 8 and 12 stainless-steel anchors.[1] The base plates were then potted with high compression-strength concrete. A foam layer separates the volumes beneath the two base plates in order to suppress direct coupling between them.

[1] Fischer FHB II-A L M16x160/100

The support structure is depicted in blue (false colors) in figure 4.1. It is a 10 m high, ca. 5000 kg heavy aluminum construction that was designed by the engineering office Heinz Berlin[2] and produced by a specialized workshop.[3] It consists of two welded aluminum assemblies bolted together by 20 BUMAX 88 M24 bolts. The lower section comprises four cylindrical feet and a 2.4 m $\times$ 2.4 m connection platform at height 3.2 m. The feet are mounted on the outer base plate through a brass and aluminum leveling mechanism that allows adjusting the tower's verticality before it is loaded with the magnetic shield. Once in place, each foot is firmly attached to the base plate with eight M20 bolts. The whole construction was approved by a structural engineering office, a necessary step given the huge lever the baseline can use to act on the base plates. The upper section is a single-piece, dual-layer aluminum construction with a small taper. The magnetic shield assembly is resting on the connection platform and attached to the tapered structure by five sets of four stainless-steel clamps that mate with the shield's frame's

[2] Ingenieur-Büro Heinz Berlin, Wennigsen, Germany

[3] Aljo Aluminium-Bau, Berne, Germany

aluminum profiles. Like the base plates and later the magnetic shield assembly, the support structure was inserted into the building in one piece by a crane, taking advantage of a sealable hatch in the roof.

Besides the dominant noise contribution from seismic activity discussed in section 3.1, mechanical factors linked to the structural construction of the apparatus can also affect a VLBAI gravimeter's accuracy and stability.

First, dynamic temperature inhomogeneities in the room hosting the apparatus lead to length variations of, mainly, the support structure, and hence height variations of the upper atomic source. At the engineering level, this imposes decoupling of the baseline pipe from the lower segment of the instrument's vacuum chamber through ultra-high vacuum bellows in order not to overstress the CF flanges along the axis. At the physical level, this is of consequence when determining the absolute position of the instrument's effective height. Depending on the thermal load in the surrounding labs and despite the running air-conditioning system, daily ambient temperature variations can reach up to 2 °C around the baseline, which, on a total height of 15 m of aluminum construction (2.3×10^{-5} /K) leads to a worst case thermal expansion of 0.7 mm. This, in-turn, corresponds to a bias of 2 nm/s^2 assuming a fixed, pre-determined, position of the instrument's effective height that does not take this effect into account. We are currently planning more advanced studies of the tower's quasi-static behavior, including precise laser-tracking of the upper chamber's height with respect to the building and correlations with ambient temperature.

Second, because the interferometry lasers are coupled from the top of the tower, transverse oscillations lead to variations of the projection of the interferometry axis (given by the light's effective wave vector k_{eff}) on local gravity. Figure 4.4 shows a typical spectrum recorded with a triaxial seismometer placed on top of the shield, at height 13.7 m (see figure 4.1). In the transverse direction, the lowest-frequency modes oscillate around 4.5 Hz and 5.5 Hz in both directions, followed by 10.4 Hz in the "East-West" direction and 12.1 Hz in the "North-South" one. These latter modes stem from oscillations of the baseline within the support structure and are displaced between the two transverse directions because the magnetic shield's frame is not constructed identically in both directions (orthogonal vs. diagonal reinforcement bars). The fundamental modes at 5.5 Hz are expected from finite-element analyses. We are currently conducting further studies to determine the character of the degenerate modes at 4.5 Hz and 5.5 Hz. From the amplitude of

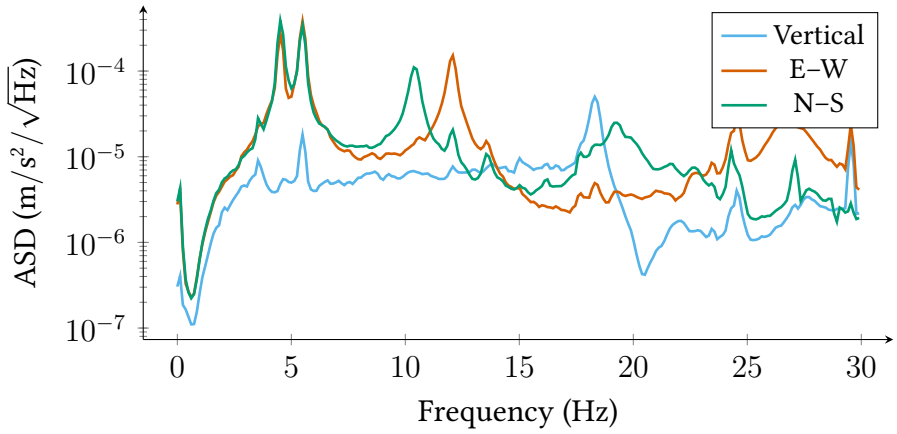

Figure 4.4: Acceleration spectral density recorded on top of the magnetic shield (height 13.7 m) with a triaxial seismometer.

the fundamental modes, we calculate a maximum displacement of around 50 µm at 5 Hz. This corresponds to a maximum vertical displacement of less than 1 nm, which is negligible. An simple estimation of transverse gravity gradients[4] is around 30 nm/s²/m, thus the corresponding change in local gravity projection is less than 3 pm/s².

[4] M. Schilling. 2020 [73]

4.2. Vacuum system

Ultracold atomic samples are fragile. In particular, the kinetic energy of a nitrogen molecule in a background gas at room temperature is vastly sufficient to kick cold atoms out of the usable sample. It is therefore essential to evacuate the baseline chamber to ultra-high vacuum (UHV), which guarantees a mean free path significantly larger than the atomic free fall distance or, equivalently, an atomic mean free travel time much longer than a typical experimental sequence. Also, beyond the pressure requirement, the engineering constraints on the baseline vacuum chamber are dictated by the required magnetic field homogeneity (see section 4.3). In particular, the chamber material must have a low and homogeneous magnetic susceptibility to avoid creating magnetic field gradients when exposed to external fields.

The baseline vacuum chamber is a 10.5 m long cylinder of outer diameter 20 cm and inner diameter 18 cm fitted with DN200 CF flanges. The material is aluminum EN AW 6061-T6, chosen for its good UHV compatibility, availability, and ease of manufacturing. To obtain a homogeneous susceptibility, the tube was extruded as a single piece, thus avoiding welding lines.[1] We limited machining contamination risks by selecting the third out of four pipes of the production batch. The flanges are bimetallic, with an aluminum

[1] Aluminiumwerk Unna AG, Unna, Germany

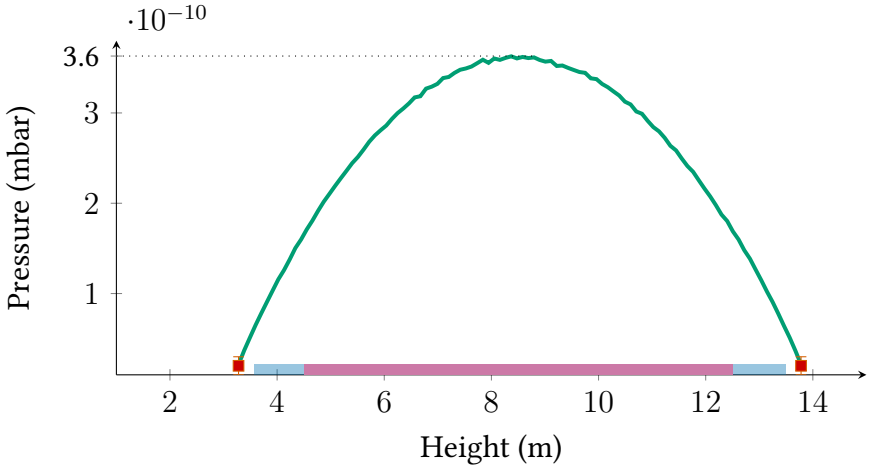

Figure 4.6: Monte-Carlo simulation of the pressure profile along the baseline axis. We measure a value of 1.5×10^{-11} mbar at both ends of the baseline pipe.

body hosting explosion-welded stainless-steel knife-edges.[2] The flanges were electron-beam welded to the raw pipe. The whole assembly was then chemically cleaned to etch away the thick and porous oxide layer formed on the inner surface during the extrusion process and reform a thin and compact one, thus reducing outgassing of the inner walls.[3] At both ends of the cylinder, modified six-way crosses host large capacity non-evaporable getter (NEG) cartridges with 3500 L/s nominal hydrogen pumping speed.[4] The whole assembly is terminated by two all-metal gate valves with DN100 CF flanges[5] (see figure 4.2).

We performed the initial pumping of the baseline vacuum chamber using two high-compression turbo-molecular pumps with nominal speed 300 L/s fitted on DN100 CF flanges and backed-up by 3.8 m^3/h membrane pumps. We baked the chamber at around 100 °C for three and a half months, until the pressure, measured at the pipe's ends, reached 2×10^{-9} mbar. The heat was delivered by three 20 m-long, 2 kW silicone isolated heating bands and the whole vacuum system was thermally insulated with 13 mm thick synthetic wool (figure 4.5). We activated the getter material at the end of the bake-out, peaking the pressure up to 1×10^{-5} mbar. After cool-down, we measured an average pressure around 1.5×10^{-11} mbar at room temperature.

Pressure measurements are only possible in the six-way crosses at the ends of the 10.5 m-long pipe. Ultra-high vacuum gauges are based on trapping ionized molecules in a magnetic field, and would therefore induce strong magnetic inhomogeneities along the baseline. The welding lines necessary to implement a CF port alone would lead to unacceptable variations in the material's magnetic permeability, and thus to spatially varying

[2] Atlas Technologies, Port Townsend, USA

[3] Assembly and cleaning by Pfeiffer Vacuum Components & Solutions GmbH, Göttingen, Germany

[4] Capacitorr D-3500, SAES Getters S.p.A, Lainate, Italy

[5] 482 Series, VAT Vakkumventile AG, Haag, Switzerland

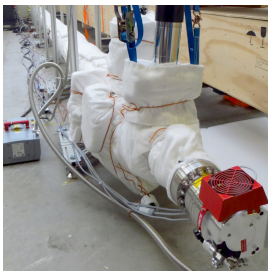

Figure 4.5: Bake-out of the baseline vacuum chamber.

magnetization. We therefore estimate the pressure profile along the baseline with a Monte-Carlo simulation powered by CERN's Molflow+ software.[6] Although the geometry is very simple, determining the parameters for the simulation is difficult because the chamber's surface quality is not well known. Following Wong,[7] we set the outgassing rate of aluminum surfaces to 3×10^{-12} mbar L/s/cm^2 and that of stainless-steel ones to 4×10^{-12} mbar L/s/cm^2. Figure 4.6 shows the resulting pressure profile, which is compatible with the measured values at the ends of the pipes and estimates a maximum pressure of 3.7×10^{-10} mbar at the center of the pipe. From the getter pump to the center, the molecular-flow conductance is

[6] R. Kersevan et al. 2019 [74]

[7] M. Wong. 2002 [75]

$$C = (12.1\,\mathrm{L/s})\frac{D^3}{L} \approx 130\,\mathrm{L/s} \tag{4.1}$$

where $D = 180$ mm is the pipe's inner diameter and $L = 5.5$ m its half length. Assuming that the residual pressure is limited by H_2, we know the nominal speed of each getter cartridge $S = 3500\,\mathrm{L/s}$ and the measured pressure at the pumps $p = 1.5 \times 10^{-11}$ mbar. The pressure in the middle of the pipe is therefore

$$\Delta P \approx \frac{pS}{C} \approx 4 \times 10^{-10}\,\mathrm{mbar} \tag{4.2}$$

which matches the result of the Monte-Carlo simulation without requiring assumptions on material outgassing rates. This shows that the surface treatment is adequate and the system is essentially conductance-limited.

Improved vacuum conditions could be reached by coating the baseline's inner walls with NEG material. This technology was developed for particle accelerators, where distributed pumping is also problematic. The coating essentially turns outgassing surfaces into pumping ones, at the expense of a higher temperature bake-out (ca. 200 °C) for activating the getter material. Unfortunately, the industry standard size for pipes is 6 m (such that two pieces can fit head-to-tail in a standard semi-trailer of length 13.6 m) and NEG coating facilities have been designed to match this length. Techniques for welding NEG coated chambers without harming the coating have been developed,[8] but are no option for our assembly since they would include a transverse welding line near the middle of the baseline. More scalable coating strategies have been developed for commercial applications but were too experimental at the time of manufacturing of our baseline vacuum chamber.[9]

[8] P. Manini et al. 2008 [76]

[9] T. Lauer et al. 2016 [77]

Imperfect vacuum leads to loss of atoms, and therefore increased noise in the atom interferometer. We can quantify this effect from the above pressure profile estimations. The collision cross-section between Rb atoms and N_2 molecules is $\sigma \approx 4 \times 10^{-18}\,\mathrm{m}^2$.[10] Assuming an ideal background gas at room temperature, a pressure of 4×10^{-10} mbar corresponds to a peak background density of $1 \times 10^{13}\,/\mathrm{m}^3$. We therefore get a minimum mean free path around 20 km, or equivalently a maximum collision frequency $f \approx 0.03\,/\mathrm{s}$. Over the course of a 2 s-long interferometer, this leads to around 6 % atom loss. This worst case estimate can be refined by taking the average mean free path over the baseline's inner 8 m, the *region of interest* (marked in pink in figure 4.6), where it approaches 40 km, which implies an atom loss of only 3 %.

[10] U. D. Rapol et al. *Phys Rev A* 64, 023402 (2001) [78]

4.3. Magnetic field control

Atoms couple to external magnetic fields through their electronic orbital (L), spin (S), and nuclear spin (I) angular momenta. In the small field regime where the energy-level shifts due to the interaction with the magnetic fields are smaller than the hyperfine splittings, the hyperfine number $F = L + S + I$ is a good quantum number. The magnetic field lifts the degeneracy between the m_F sub-levels and the dominant effect is the anomalous Zeeman effect, proportional to m_F. The Breit–Rabi formula[1] describes corrections to the Zeeman effect for $J = 1/2$ states (namely the ground states of alkali elements):[2,3]

[1] G. Breit et al. *Phys Rev* 38, 2082 (1931) [79]

[2] D. A. Steck. 2019 [80]

[3] M. Meister. 2020 [81]

$$\Delta E = C_1 m_F B \pm \frac{\Delta E_{\mathrm{HFS}}}{2}\sqrt{1 + C_2 m_F B + C_3 B^2} \tag{4.3}$$

where $\{C_j\}$ are constants and ΔE_{HFS} is the hyperfine splitting. To avoid direct contributions from the anomalous Zeeman effect, precision atom-interferometry experiments typically operate with polarized $m_F = 0$ samples. Developed to second-order in B, the Breit–Rabi formula reduces to:

$$\Delta E = \frac{(g_J - g_I)^2 \mu_B^2}{2\Delta E_{\mathrm{HFS}}} B^2 \equiv \frac{1}{2}\hbar\alpha B^2 \tag{4.4}$$

where g_J, g_I are the electronic and nuclear g-factors, μ_B is the Bohr magneton, and we rewrote the constant C_3 in terms of physical properties of the system. The constant α is usually called "clock Zeeman coefficient" since it quantifies the Zeeman shift for $m_F = 0$ "clock" states. This energy landscape gives rise to a spurious force proportional to its negative gradient.

The derivation above delivers the two key aspects of magnetic field control for atom interferometry. On the one hand, a quantization axis must be realized, such that the eigenstates with eigenvalues m_F are well-defined. This field must be much larger than any local variation, to avoid depolarizing the atomic sample. On the other hand, the spurious force is locally proportional to $\partial B^2 \propto B\partial B$ and thus both the field magnitude and its gradients should be minimized.

The quantization field is realized with a solenoid supported by the baseline's cylindrical vacuum chamber. The coil's inner diameter is therefore 20 cm. We used square cross-section wire[4] to ensure good stacking of the windings and minimize gaps. The choice of wire thickness is a compromise between field quality and practicability, since the solenoid needs to span the full baseline length, *i.e.*, 10.5 m. We chose a thickness $w = 2.5\,\mathrm{mm}$, which leads to a maximum winding density $n = 400\,/\mathrm{m}$ and maximum wire length of 2640 m. The copper core is electrically insulated by a polyimide film of nominal thickness 0.15 mm wrapped with approximately 50 % overlap. This leads to an effective wire thickness $w' = 3.1\,\mathrm{mm}$ and density $n' \approx 323\,/\mathrm{m}$. The total resistance is on the order of 10 Ω. The generated field is then 0.4 µT/mA and the thermal dissipation less than 0.1 mW/µT^2. Figure 4.7 shows the winding operation. The non-evacuated vacuum chamber was positioned on five pairs of inflated wheels and rotated using a large handle mounted on one of the end flanges. The insulated copper wire is fed sideways under tension. This task was fulfilled within two working days by two persons.

[4] Gebauer & Griller Kabelwerke GesmbH, Vienna, Austria

Figure 4.7: Winding of the quantization field solenoid.

The baseline vacuum chamber and solenoid are enclosed in the high performance magnetic shield described in our article.[5] The shield serves two purposes. First, it reduces the magnitude of the magnetic field along the baseline, thus allowing the use of a small bias field. This not only constrains the clock Zeeman shift, but also helps the baseline's thermal design. Second, it creates a highly homogeneous magnetic environment, thus also limiting the Zeeman-associated systematic effect. Cross-talk between the shield and the solenoid has not been explicitly tested and is in principle hard to predict. However, since the solenoid generates a field parallel to the shield's weak axis, it is unlikely that it magnetizes adversely the high permeability material. We therefore assume that we can simply add up the solenoid field and the shield's residual field when evaluating the clock Zeeman shift along the baseline.

[5] E. Wodey et al. *Rev Sci Instrum* 91, 035117 (2020) [82]

Owing to the sub 5 nT residual field from the magnetic shield along the central 8 m of the baseline, quantization fields of 500 nT and below can be considered. This is factor 5 better than

the 2.5 µT envisaged when calculating first parameters for this instrument.[6] With the winding density $n' = 323\,/\mathrm{m}$, this requires a current of 1.2 mA and dissipates 15 µW, which is insignificant when distributed across the baseline vacuum chamber's outer surface.

[6] J. Hartwig et al. *New J Phys* 17, 035011 (2015) [21]

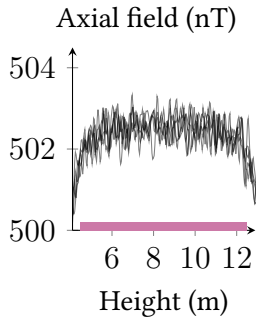

Figure 4.8: Randomized simulation of the effect of imperfect wiring on the solenoid field for a current of 1.24 mA.

The necessarily imperfect wiring of the solenoid leads to spurious magnetic field gradients. We estimate this effect using a randomized simulation. The wiring gaps are distributed according to a skew-normal distribution with skewness $\alpha = 5$, location $\xi = 0.3\,\mathrm{mm}$, and scale $\omega = 1\,\mathrm{mm}$. We chose a skewed distribution to minimize nonphysical negative gap sizes while keeping the simulation reasonably simple. The parameters are educated guesses based on a qualitative observation of the finished solenoid. Figure 4.8 shows five realizations of the random model, which result in peak-to-peak variations of the field around 2 nT, comparable to the amplitude of the magnetic shield's residual field. The high spatial frequency mirrors the solenoid's high winding density. In addition, we anticipate current noise not to be an issue for sources in the mA range where noise densities well below $10\,\mathrm{nA}/\sqrt{\mathrm{Hz}}$ in the few Hz band are easily available, even as ready-made integrated circuits.

Applying perturbation theory[7] to the combined solenoid and shield residual fields on the reference interferometer, we obtain a Zeeman effect-related acceleration bias smaller than $5 \times 10^{-14}\,\mathrm{m/s^2}$, dominated by the shield's residual field contribution. This occurs thanks to the interferometer's spatial averaging behavior and confirms that the solenoid winding quality should not limit the instrument's accuracy when operated at the field levels considered here.

[7] C. Ufrecht et al. *Phys Rev A* 101, 053615 (2020) [72]

4.4. Temperature monitoring

The finite temperature of the baseline's vacuum chamber leads to black-body radiation which interacts with the atomic sample. As shown by Haslinger *et al.*,[1] the dominant effect is not radiation pressure but the attractive force due to the atomic polarizability. For a local temperature $T(z)$, the black-body radiation potential reads

[1] P. Haslinger et al. *Nat Phys* 14, 257 (2018) [83]

$$V(z) = -2\frac{\alpha_X \sigma T^4(z)}{c\epsilon_0} \tag{4.5}$$

where α_X is the atomic polarizability, σ the Stefan–Boltzmann constant, c the speed of light in vacuum, and ϵ_0 the vacuum permittivity. The resulting local acceleration is therefore

proportional to the local temperature gradient and the cube of the absolute local temperature.

Haslinger *et al.* point out that the effect can be significant even for seemingly benign temperature gradients. For example, given an atomic polarizability $\alpha_{\mathrm{Rb}} = h \cdot 0.08\,\mathrm{Hz/V^2\,cm^2}$, ^{87}Rb atoms would experience an acceleration of more than 10 pm/s^2 in a gradient of 100 mK/m around 20 °C. Unfortunately, such gradients can in principle occur very easily on large devices, thus requiring monitoring accurate to the sub-100 mK level.

The only practical location along the baseline accessible to thermometers is the outer surface of the bias solenoid. Since this surface is inside the magnetic shielding, one needs to ensure that the full assembly is not magnetizable, in order not to create magnetic field inhomogeneities. Figure 4.9 shows the sensor assembly. It consists of a Pt-1000 resistor with pure silver leads[2] soldered to a double twisted-pair Cu cable. We used a $Sn_{60}PbCu_2$ soldering wire. This avoids the nickel components used in usual lead-free soldering compounds. We found the wetting behavior of alternative SnAgCu alloys unsatisfactory. The double twisted-pair cable type is LiYCY-P AWG 24 (0.25 mm^2), featuring a PVC isolation and a single braided shield. The pair colors are yellow/green and white/brown for the excitation and the sense channels respectively. The cable is strapped to the baseline pipe using 10 mm-wide nylon cable ties. Thermal contacting is provided by a silver and ceramics-based thermal compound. The sensitive volume is potted with two-component epoxy for long-term stability.

[2] IST AG, Ebnat-Kappel, Switzerland

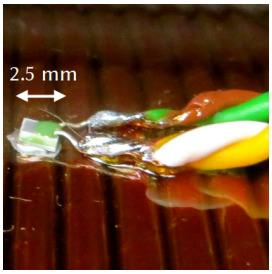

Figure 4.9: Non-magnetic Pt-1000 thermometer assembly.

We evaluated the magnetization properties of the thermometry setup using the SQUID array of the Berlin magnetically shielded room 2 (BMSR-2) at the PTB in Berlin.[3] Prior to screening, we exposed each sample to a 30 mT field. For the sensors, we only tested samples, including different soldering alloy options. We screened the full 300 m of cable used, rejecting segments showing more than 50 pT remanence at 4 cm distance.

[3] S. Bechstein et al. *J Phys: Conf Ser* 43, 309 (2006) [84]

The Pt-1000 elements are specified according to 1/10 DIN EN 60751, that is a manufacturing inaccuracy of ±30 mK from 25 °C to 55 °C. The nominal resistance is $R_0 = 1\,\mathrm{k\Omega}$ at $T_0 = 0\,^\circ\mathrm{C}$ and the temperature coefficient is $\alpha_0 = 3.85 \times 10^{-3}\,/\mathrm{K}$. Readout errors are minimized using a 4-point method. With an excitation current $I_0 = 200\,\mu\mathrm{A}$, the readout sensitivity is 770 µV/K, *i.e.* the voltage readout accuracy needs to be better than 25 µV (referred to the input) to obtain a temperature readout accuracy at the 30 mK level. This is challenging. For example, the common instrumentation amplifier LT1167[4] has worst case 50 µV voltage

[4] Linear Technology Corp. 1998 [85]

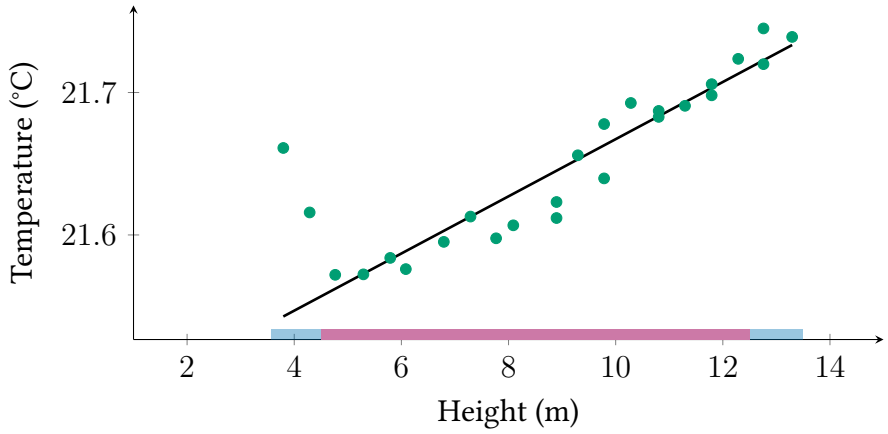

Figure 4.10: Least-squares adjusted temperature measurement network. The overall gradient is 20 mK/m.

offset (RTI) for a gain of 20. Chopped-architectures are more suited with a worst case 20 µV offset for the AD8230 chip[5] but this scenario still requires careful characterization of the individual offsets.

[5] Analog Devices Inc. 2004 [86]

Instead of a lumped design, we opted for the integrated MAX31865[6] solution. We compensate for the accuracy of only 0.5 °C by using a single converter and iteratively building a network of connected measurements between sensors. This is valid since we don't expect the local temperatures to vary significantly on the 10 s time scale. A least-squares adjustment[7] of the graph provides a best estimate for the temperature differences between the nodes. There are in total 30 sensors distributed along the baseline in 50 cm spacing with redundancy every meter. Figure 4.10 shows the adjusted temperature network measured in typical lab conditions. No optimizations of the air-conditioning system have been performed, such that the result does not rely on tedious and environment-dependent parameter tuning. The magnetic shield (including it's wooden support) also shields the baseline pipe from fast temperature variations in the laboratory. The adjusted uncertainty is 14 mK per point. We observe an overall gradient of 20 mK/m around a temperature of 21.65 °C. For rubidium 87 atoms, the bias acceleration corresponding to the potential in equation 4.5 amounts to 3×10^{-12} m/s^2.

[6] Maxim Integrated Products Inc. 2015 [87]

[7] C. D. Ghilani. Wiley, 2017. Chap. 12 [88]

5. Summary & Outlook

Towards VLBAI gravimetry

In this manuscript, we introduced the very long baseline atom interferometry facility in Hannover. We motivated the associated physical and technical developments by its applicability in high-accuracy gravimetry. We discussed the well-known principles of atomic gravimetry to review the key promises of very long baseline atomic gravimeters, especially in terms of their measurement sensitivity. However, the same considerations lead to severe challenges linked to the use of an extended baseline. Besides the control of the atomic wave packets, only the fast creation of large cold atomic samples coupled with careful engineering and precise characterization of the instrument's environment can offer prospects for reaching the sub-nm/s^2 accuracy in atomic gravimetry. We showed in particular that the projected biases of the Hannover VLBAI facility operated as a ^{87}Rb gravimeter are not limited by its engineering. Below, we summarize the considered effects and give upper bounds to the associated biases derived from the presented characterization measurements:

Baseline mechanical oscillations Bias $\lesssim 3\,\mathrm{pm/s^2}$;
Baseline thermal expansion Bias $\lesssim 2\,\mathrm{nm/s^2}$. This is a worst case estimate. Preliminary data from a laser tracking campaign shows control of this bias well below the $1\,\mathrm{nm/s^2}$ level thanks to the temperature stability of the labs;
Magnetic field variations Bias $\lesssim 0.1\,\mathrm{pm/s^2}$;
Temperature inhomogeneity Bias $\lesssim 5\,\mathrm{pm/s^2}$.

In the future, improvements of the instrument's environmental and self-gravity models discussed in section 3.2 will pave the way towards comparisons of a VLBAI gravimeter with other, transportable, instruments at the sub-10 nm/s^2 level. We also envisage VLBAI instruments to take advantage of their great versatility in measuring different inertial quantities (gravity, gravity gradients, rotations) and form networks with other similar

instruments to realize quantum geodetic Earth observatories. An example application could for example be Earthquake early detection systems.[1]

[1] T. Shimoda et al. *Geophys J Int* 224, 533 (2021) [89]

Complementary research directions

Absolute gravimetry is only one of many research areas targeted by the Hannover VLBAI facility. The availability of such high-performance devices creates a variety of opportunities for fundamental physics research. Originally, the motivation for the project in Hannover is testing the universality of free fall with the atomic species rubidium and ytterbium. Following the first atomic test of the universality of free fall with two different chemical species (^{87}Rb and ^{39}K),[2] realistic parameters for a test at the 10^{-13} level and beyond with ^{170}Yb and ^{87}Rb were calculated.[3] Here, the use of the ytterbium atom provides complementary sensitivity to the Rb/K pair when interpreting the results in the context of standard model extensions.[4] The intrinsic isotopic purity and variety of possible cold atoms test masses combinations allows to test multiple violation scenarios. This is a major advantage of atomic tests compared to the currently better performing classical tests, like the leading result from the MICROSCOPE satellite mission.[5] The group operating the Stanford fountain recently published a test at the 10^{-12} level between two rubidium isotopes.[6] Other groups have compared the free fall of identical atoms in different energy states or even coherent superpositions of such states.[7] The field is however still very open for tests with different chemical species at levels competing and surpassing the best classical tests.

[2] D. Schlippert et al. *Phys Rev Lett* 112, 203002 (2014) [90]

[3] J. Hartwig et al. *New J Phys* 17, 035011 (2015) [21]

[4] M. A. Hohensee et al. *Phys Rev Lett* 111, 151102 (2013) [91]

[5] P. Touboul et al. *Phys Rev Lett* 119, 231101 (2017) [8]

[6] P. Asenbaum et al. *Phys Rev Lett* 125, 191101 (2020) [14]

[7] G. Rosi et al. *Nat Commun* 8, 15529 (2017) [92]

Large scale quantum experiments are always intriguing, as they confront the most spectacular features of quantum mechanics, for example the superposition principle, with our experience of the macroscopic world. Following-up on the pioneering work in Stanford where a coherent superposition of rubidium momentum states with a maximum separation of 50 cm was demonstrated,[8] the Hannover VLBAI facility offers a platform for macroscopic superposition tests over 8 m with bodies up to 176 atomic mass units. Trading mass for distance, such experiments would advantageously complement results from large molecular interferometry.[9] Techniques required to produce such de-localized quantum superposition states include very large momentum transfer beam splitters and precise control of the wave packet expansion. This research program therefore integrates well into that targeting enhanced absolute gravimetry and tests of the universality of free fall.

[8] T. Kovachy et al. *Nature* 528, 530 (2015) [93]

[9] B. Schrinksi et al. *Phys Rev Research* 2, 033034 (2020) [94]

The possibilities opened by the inclusion of ytterbium as an atomic species for the Hannover VLBAI facility are not limited to improved tests of the universality of free fall. The bosonic isotopes feature zero nuclear spin, such that the zero electronic angular momentum ground state ($^1S_0$) has no hyperfine fine structure. This allows anticipating much lower couplings to external electromagnetic fields than those calculated for rubidium atoms in chapter 4. In addition, like other alkaline-earth-like atoms (e.g. Mg, Ca, Sr, Cd, Hg) used for optical lattice clocks, the availability of an ultra-narrow transition, and the associated metastable excited state, allow for single-photon beam splitters,[10] a key technique for future atomic gravitational wave detectors.[11]

Introducing clocks in very long baseline atom interferometry extends the probe of the interface between quantum mechanics and general relativity even further than atomic tests of the universality of free fall. It has been observed that sending ticking clocks along interferometric paths at different heights, so different gravitational potentials and therefore time dilations, should lead to which-path information and therefore loss of interferometric contrast.[12] This naturally leads to the question whether it would be possible to use this effect to test the universality of the gravitational redshift with atom interferometry beyond the seminal results from the Gravity Probe A mission.[13] In the context of the work presented here, we contributed to the development of the concept of quantum clocks, and proposed an implementation of the well-known twin paradox in special relativity based on atom interferometry.[14] Further developments have lead to concrete proposals for testing the universality of gravitational redshift with VLBAI,[15] although without the controverted increase in sensitivity at the heart of the so-called "redshift debate".[16] Nevertheless, quantum clocks add to absolute gravimetry, macroscopic massive de-localizations, and tests of the universality of free fall to form very long baseline atom interferometry's overarching research agenda: exploring quantum systems in gravity.

[10] L. Hu et al. *Phys Rev Lett* 119, 263601 (2017) [95]

[11] N. Yu et al. *Gen Relat Gravit* 43, 1943 (2011) [96]

[12] M. Zych et al. *Nat Commun* 2, 505 (2011) [97]

[13] R. F. C. Vessot et al. *Phys Rev Lett* 45, 2081 (1980) [98]

[14] S. Loriani et al. *Sci Adv* 5, eaax8966 (2019) [99]

[15] C. Ufrecht et al. *Phys Rev Research* 2, 043240 (2020) [100]

[16] W. P. Schleich et al. *Phys Rev Lett* 110, 010401 (2013) [101]

Author contributions

The following list contains the publications linked to the contents of this manuscript, ordered by publication date. All the listed articles are published under open-access licenses. The corresponding author contributions statement was copied from the published version where applicable.

1. S. Loriani, A. Friedrich, C. Ufrecht, F. Di Pumpo, S. Kleinert, S. Abend, N. Gaaloul, C. Meiners, C. Schubert, D. Tell, **E. Wodey**, M. Zych, W. Ertmer, A. Roura, D. Schlippert, W. P. Schleich, E. M. Rasel, and E. Giese
   Interference of Clocks: A Quantum Twin Paradox
   Science Advances 5, eaax8966, 2019
   DOI: 10.1126/sciadv.aax8966

   All authors contributed to scientific discussions, the execution of the study, and the interpretation of the results. S. L. and A. F. contributed equally to this work. S.L., A.F., C.U., F.D.P., and E.G. prepared the manuscript with input from S.K., S.A., N.G., C.M., D.T., E.W., M.Z., W.E., A.R., D.S. as well as E.M.R and W.P.S. E.M.R, W.P.S, and E.G. supervised the project.

2. **E. Wodey**, D. Tell, E. M. Rasel, D. Schlippert, R. Baur, U. Kissling, B. Kölliker, M. Lorenz, M. Marrer, U. Schläpfer, M. Widmer, C. Ufrecht, S. Stuiber, and P. Fierlinger
   A scalable high-performance magnetic shield for Very Long Baseline Atom Interferometry
   Review of Scientific Instruments 91, 035117, 2020
   DOI: 10.1063/1.5141340

   P.F., S.S., M.W., and U.S. designed the shield based on input from E.W, D.T., E.M.R, and D.S. R.B. and M.M. assembled the shield with support from U.K., B.K., M.L., U.S., and M.W. E.W., M.L., S.S., and P.F. developed the specific equilibration procedure. E.W., M.L., U.K., B.K. and D.S. carried out the measurements with support from R.B., M.M., and U.S. E.W. and C.U. evaluated the effect of the residual field on atom interferometers. E.W. prepared the manuscript with input from all authors. E.M.R. and D.S. supervised the project.

3. M. Schilling, **E. Wodey**, L. Timmen, D. Tell, K. H. Zipfel, D. Schlippert, C. Schubert, E. M. Rasel, and J. Müller
Gravity field modelling for the Hannover 10 m atom interferometer
Journal of Geodesy 94, 122, 2020
DOI: 10.1007/s00190-020-01451-y

M.S., E.W., and L.T. planned geometric and gravimetric measurements, evaluated the data and prepared the initial draft. E.W., D.T., D.S., C.S., and E.M.R. conceptualized the VLBAI instrument. E.W, D.T, and K.H.Z. designed and built the measurement platforms. M.S., E.W., L.T., D.T., and K.H.Z. carried out the measurements. M.S. developed and implemented the gravity model. D.T., K.H.Z., D.S., C.S, E.M.R., and J.M. provided critical input to the manuscript.

4. L. L. Richardson, A. Rajagopalan, H. Albers, C. Meiners, D. Nath, C. Schubert, D. Tell, **E. Wodey**, S. Abend, M. Gersemann, W. Ertmer, E. M. Rasel, D. Schlippert, M. Mehmet, L. Kumanchik, L. Colmenero, R. Spannagel, C. Braxmaier, and F. Guzmán
Optomechanical resonator-enhanced atom interferometry
Communications Physics 3, 208, 2020
DOI: 10.1038/s42005-020-00473-4

W.E., E.M.R., C.S., and D.S. designed the atom interferometer and its laser system. L.L.R., H.A., D.N., and D.S. contributed to the design of the atom interferometer and its laser system and realized the overall setup. A.R., M.M., L.K., L.C., R.S., C.B., and F.G. designed, built, and tested the optomechanical resonator and designed the readout laser system. A.R., C.M., D.T., and E.W. built and characterized the laser system for readout. L.L.R., F.G., L.K., and A.R. implemented the optomechanical resonator in the atom interferometer setup. L.L.R., H.A., D.N., and A.R. operated the final experimental setup. Sv.A., M.G., and C.S. contributed to the data acquisition system utilized for post correction. A.R., D.N., C.S., and L.L.R. performed the analysis of the data presented in this manuscript. L.L.R., D.S., and F.G. drafted the initial manuscript. A.R., C.M., C.S., D.T., E.W., E.M.R., and L.K. provided major input to the manuscript and all authors critically reviewed and approved of the final version.

5. **E. Wodey**, R. J. Rengelink, C. Meiners, E. M. Rasel, and D. Schlippert
A robust, high-flux source of laser-cooled ytterbium atoms
Journal of Physics B: Atomic, Molecular, and Optical Physics 54, 035301, 2021
DOI: 10.1088/1361-6455/abd2d1

E.W., C.M., E.M.R, and D.S. designed the vacuum system and the ytterbium oven. E.W. designed and assembled the permanent magnet Zeeman slower. R.R. developed the laser system and commissioned the apparatus. E.W and R.R. carried out, analyzed, and interpreted the measurements. E.W. and R.R. prepared the initial draft. All authors critically reviewed the manuscript. E.M.R and D.S. supervised the project.

Bibliography

[1] A. D. Ludlow, M. M. Boyd, J. Ye, E. Peik, and P. O. Schmidt. Optical atomic clocks. *Rev Mod Phys* 87, 637 (2015).

[2] L. Morel, Z. Yao, P. Cladé, and S. Guellati-Khélifa. Determination of the fine-structure constant with an accuracy of 81 parts per trillion. *Nature* 588, 61 (2020).

[3] G. Rosi, F. Sorrentino, L. Cacciapuoti, M. Prevedelli, and G. M. Tino. Precision measurement of the Newtonian gravitational constant using cold atoms. *Nature* 510, 518 (2014).

[4] M. S. Safronova et al. Search for new physics with atoms and molecules. *Rev Mod Phys* 90, 025008 (2018).

[5] M. Travagnin. Cold atom interferometry for inertial navigation sensors. *JRC Tech Rep*, EUR 30492 (2020).

[6] K. Wright et al. Benchmarking an 11-qubit quantum computer. *Nat Commun* 10, 5464 (2019).

[7] P. Gillot, O. Francis, A. Landragin, F. P. D. Santos, and S. Merlet. Stability comparison of two absolute gravimeters: optical versus atomic interferometers. *Metrologia* 51, L15 (2014).

[8] P. Touboul et al. MICROSCOPE Mission: First Results of a Space Test of the Equivalence Principle. *Phys Rev Lett* 119, 231101 (2017).

[9] H. Müller, S.-w. Chiow, Q. Long, S. Herrmann, and S. Chu. Atom Interferometry with up to 24-Photon-Momentum-Transfer Beam Splitters. *Phys Rev Lett* 100, 180405 (2008).

[10] F. Anders et al. Momentum Entanglement for Atom Interferometry (2020). arXiv: 2010.15796 [quant-ph].

[11] B. Canuel et al. Exploring gravity with the MIGA large scale atom interferometer. *Sci Rep* 8, 14064 (2018).

[12] L. Badurina et al. AION: an atom interferometer observatory and network. *J Cosmol Astropart P* 5, 11 (2020).

[13] M. Abe et al. Matter-wave Atomic Gradiometer Interferometric Sensor (MAGIS-100) (2021). arXiv: 2104.02835 [physics.atom-ph].

[14] P. Asenbaum, C. Overstreet, M. Kim, J. Curti, and M. A. Kasevich. Atom-Interferometric Test of the Equivalence Principle at the 10^{-12} Level. *Phys Rev Lett* 125, 191101 (2020).

[15] I. Marson and J. E. Faller. g – the acceleration of gravity: its measurement and its importance. *J Phys E: Sci Instrum* 19, 22 (1986).

[16] J. Grotti et al. Geodesy and metrology with a transportable optical clock. *Nat Phys* 14, 437 (2018).
[17] K. U. Schreiber et al. The large ring laser G for continuous Earth rotation monitoring. *Pure Appl Geophys* 166, 1485 (2009).
[18] M. Van Camp et al. Geophysics from terrestrial time-variable gravity measurements. *Rev Geophys* 55, 938 (2017).
[19] P. Asenbaum et al. Phase shift in an atom interferometer due to spacetime curvature across its wave function. *Phys Rev Lett* 118, 183602 (2017).
[20] J. Lautier et al. Hybridizing matter-wave and classical accelerometers. *Appl Phys Lett* 105, 144102 (2014).
[21] J. Hartwig et al. Testing the universality of free fall with rubidium and ytterbium in a very large baseline atom interferometer. *New J Phys* 17, 035011 (2015).
[22] J. M. Goodkind. The superconducting gravimeter. *Rev Sci Instrum* 70, 4131 (1999).
[23] M. Van Camp, O. Francis, and T. Lecocq. Recording Belgium's gravitational history. *Eos* 98 (2017).
[24] T. M. Niebauer, G. S. Sasagawa, J. E. Faller, R. Hilt, and F. Klopping. A new generation of absolute gravimeters. *Metrologia* 32, 159 (1995).
[25] M. Bilker-Koivula, J. Mäkinen, H. Ruotsalainen, J. Näränen, and T. Saari. Forty-three years of absolute gravity observations of the Fennoscandian postglacial rebound in Finland. *J Geodesy* 95, 24 (2021).
[26] V. Pálinkáš, H. Wziontek, M. Vaľko, P. Křen, and R. Falk. Evaluation of comparisons of absolute gravimeters using correlated quantities: reprocessing and analyses of recent comparisons. *J Geodesy* 95, 21 (2021).
[27] M. A. Kasevich and S. Chu. Atomic interferometry using stimulated Raman transitions. *Phys Rev Lett* 67, 181 (1991).
[28] A. Peters, K. Y. Chung, and S. Chu. High-precision gravity measurements using atom interferometry. *Metrologia* 28, 25 (2001).
[29] C. Freier et al. Mobile quantum gravity sensor with unprecedented stability. *J Phys: Conf Ser* 723, 012050 (2016).
[30] D. Carbone et al. The NEWTON-g Gravity Imager: Toward New Paradigms for Terrain Gravimetry. *Front Earth Sci* 8, 573396 (2020).
[31] J. E. Faller. Thirty years of progress in absolute gravimetry: a scientific capability implemented by technological advances. *Metrologia* 39, 425 (2002).
[32] R. Karcher, A. Imanaliev, S. Merlet, and F. Pereira Dos Santos. Improving the accuracy of atom interferometers with ultracold sources. *New J Phys* 20, 113041 (2018).
[33] N. Heine et al. A transportable quantum gravimeter employing delta-kick collimated Bose–Einstein condensates. *Eur Phys J D* 74, 174 (2020).
[34] R. Colella, A. W. Overhauser, and S. A. Werner. Observation of Gravitationally Induced Quantum Interference. *Phys Rev Lett* 34, 1472 (1975).
[35] J. M. Hogan, D. M. S. Johnson, and M. A. Kasevich. Light-pulse atom interferometry (2008). arXiv: `0806.3261 [physics.atom-ph]`.
[36] C. Antoine and C. J. Bordé. Quantum theory of atomic clocks and gravito-inertial sensors: an update. *J Opt B - Quantum S O* 5, S199 (2003).

[37] A. M. Nobili, A. Anselmi, and R. Pegna. Systematic errors in high-precision gravity measurements by light-pulse atom interferometry on the ground and in space. *Phys Rev Research* 2, 012036 (2020).
[38] J. Rappaz and M. Picasso. Introduction à l'analyse numérique. Presses polytechniques et universitaires romandes, Lausanne, 2010.
[39] J. F. Clauser. Ultra-high sensitivity accelerometers and gyroscopes using neutral atom matter-wave interferometry. *Physica B* 151, 262 (1988).
[40] T. M. Niebauer et al. Simultaneous gravity and gradient measurements from a recoil-compensated absolute gravimeter. *Metrologia* 48, 154 (2011).
[41] P. Storey and C. Cohen-Tannoudji. The Feynman path integral approach to atomic interferometry. A tutorial. *J Phys II France* 4, 1999 (1994).
[42] C. Schubert et al. Multi-loop atomic Sagnac interferometry (2021). arXiv: 2102.00991 [physics.atom-ph].
[43] L. A. Sidorenkov, R. Gautier, M. Altorio, R. Geiger, and A. Landragin. Tailoring Multiloop Atom Interferometers with Adjustable Momentum Transfer. *Phys Rev Lett* 125, 213201 (2020).
[44] W. Ketterle. Nobel lecture: When atoms behave as waves: Bose-Einstein condensation and the atom laser. *Rev Mod Phys* 74, 1131 (2002).
[45] C.-C. Chen, S. Bennetts, R. G. Escudero, B. Pasquiou, and F. Schreck. Continuous Guided Strontium Beam with High Phase-Space Density. *Phys Rev Applied* 12, 044014 (2019).
[46] J. Rudolph et al. A high-flux BEC source for mobile atom interferometers. *New J Phys* 17, 065001 (2015).
[47] G. J. Dick. Local oscillator instabilities in trapped ion frequency standards. *19th Annual Precise Time and Time Interface Systems and Applications Meeting, Redondo Beach, California*. 1987.
[48] D. Savoie et al. Interleaved atom interferometry for high-sensitivity inertial measurements. *Sci Adv* 4, eaau7948 (2018).
[49] P. Cheinet, B. Canuel, A. Gauguet, F. Yver-Leduc, and A. Landragin. Measurement of the Sensitivity Function in a Time-Domain Atomic Interferometer. *IEEE T Instrum Meas* 57, 1141 (2008).
[50] E. Wodey, R. J. Rengelink, C. Meiners, E. M. Rasel, and D. Schlippert. A robust, high-flux source of laser-cooled ytterbium atoms. *J Phys B: At Mol Opt Phys* 54, 035301 (2021).
[51] P. Cladé, S. Guellati-Khélifa, F. Nez, and F. Biraben. Large Momentum Beam Splitter Using Bloch Oscillations. *Phys Rev Lett* 102, 240402 (2009).
[52] H. Müller, S.-w. Chiow, S. Herrmann, and S. Chu. Atom Interferometers with Scalable Enclosed Area. *Phys Rev Lett* 102, 240403 (2009).
[53] H. Müntinga et al. Interferometry with Bose-Einstein Condensates in Microgravity. *Phys Rev Lett* 110, 093602 (2013).
[54] D. Becker et al. Space-borne Bose–Einstein condensation for precision interferometry. *Nature* 562, 391 (2018).
[55] T. Kovachy et al. Matter Wave Lensing to Picokelvin Temperatures. *Phys Rev Lett* 114, 143004 (2015).
[56] M. Schilling et al. Gravity field modelling for the Hannover 10 m atom interferometer. *J Geodesy* 94, 122 (2020).

[57] P. Cladé et al. A promising method for the measurement of the local acceleration of gravity using Bloch oscillations of ultracold atoms in a vertical standing wave. *Europhys Lett* 71, 730 (2005).
[58] R. Charrière, M. Cadoret, N. Zahzam, Y. Bidel, and A. Bresson. Local gravity measurement with the combination of atom interferometry and Bloch oscillations. *Phys Rev A* 85, 013639 (2012).
[59] V. Xu et al. Probing gravity by holding atoms for 20 seconds. *Science* 366, 745 (2019).
[60] S. Abend et al. Atom-Chip Fountain Gravimeter. *Phys Rev Lett* 117, 203003 (2016).
[61] M. Andia et al. Compact atomic gravimeter based on a pulsed and accelerated optical lattice. *Phys Rev A* 88, 031605 (2013).
[62] Z.-K. Hu et al. Demonstration of an ultrahigh-sensitivity atom-interferometry absolute gravimeter. *Phys Rev A* 88, 043610 (2013).
[63] J. Peterson. Observations and Modeling of Seismic Background Noise. *U.S. Geological Survey open-file report* 93, 322 (1993).
[64] M. G. Beker et al. Seismic Attenuation Technology for the Advanced Virgo Gravitational Wave Detector. *2nd Internation Conference on Technology and Instrumentation in Particle Physics (TIPP'11), Chicago, USA*. 2012.
[65] G. Bergmann. Improving the seismic isolation for the AEI 10 m prototype. PhD thesis. Hannover: Leibniz Universität Hannover, 2018.
[66] V. Ménoret et al. Gravity measurements below $10^{-9}g$ with a transportable absolute quantum gravimeter. *Sci Rep* 8, 1 (2018).
[67] O. Gerberding, F. Guzmán Cervantes, J. Melcher, J. R. Pratt, and J. M. Taylor. Optomechanical reference accelerometer. *Metrologia* 52, 654 (2015).
[68] L. L. Richardson, A. Hines, A. Schaffer, B. P. Anderson, and F. Guzmán. Quantum hybrid optomechanical inertial sensing. *Appl Optics* 59, G160 (2020).
[69] L. L. Richardson et al. Optomechanical resonator-enhanced atom interferometry. *Commun Phys* 3, 208 (2020).
[70] C. Overstreet, P. Asenbaum, and M. A. Kasevich. Physically relevant phase shifts in matter-wave interferometry. *Am J Phys* 89, 324 (2021).
[71] G. D'Agostino, S. Merlet, A. Landragin, and F. Pereira Dos Santos. Perturbations of the local gravity field due to mass distribution on precise measuring instruments: a numerical method applied to a cold atom gravimeter. *Metrologia* 48, 299 (2011).
[72] C. Ufrecht and E. Giese. Perturbative operator approach to high-precision light-pulse atom interferometry. *Phys Rev A* 101, 053615 (2020).
[73] M. Schilling. private communication. 2020.
[74] R. Kersevan and M. Ady. Recent Developments of Monte-Carlo Codes Molflow+ and Synrad+. *10th Int. Particle Accelerator Conf. (IPAC'19), Melbourne, Australia*. 2019.
[75] M. Wong. *Review of papers regarding vacuum system and materials*. 2002. URL: https://home.fnal.gov/~mlwong/outgas_rev.htm (visited on 01/08/2021).
[76] P. Manini et al. NEG Coated Chambers at SOLEIL: Technological Issues and Experimental Results. *11th European Particle Accelerator Conf. (EPAC'08), Genoa, Italy*. 2008.
[77] Vacuum apparatus and method for coating components. T. Lauer and A. Kraft. 2016.

[78] U. D. Rapol, A. Wasan, and V. Natarajan. Loading of a Rb magneto-optic trap from a getter source. *Phys Rev A* 64, 023402 (2001).
[79] G. Breit and I. I. Rabi. Measurement of Nuclear Spin. *Phys Rev* 38, 2082 (1931).
[80] D. A. Steck. *Rubidium 87 D Line Data*. 2019. URL: http://steck.us/alkalidata (visited on 12/15/2020).
[81] M. Meister. private communication. 2020.
[82] E. Wodey et al. A scalable high-performance magnetic shield for Very Long Baseline Atom Interferometry. *Rev Sci Instrum* 91, 035117 (2020).
[83] P. Haslinger et al. Attractive force on atoms due to blackbody radiation. *Nat Phys* 14, 257 (2018).
[84] S. Bechstein et al. Digitally controlled high-performance dc SQUID readout electronics for a 304-channel vector magnetometer. *J Phys: Conf Ser* 43, 309 (2006).
[85] Linear Technology Corp. *LT1167 – Single Resistor Gain Programmable, Precision Instrumentation Amplifier*. 1998. URL: https://www.analog.com/en/products/lt1167.html (visited on 12/11/2020).
[86] Analog Devices Inc. *AD8230 – Rail-to-Rail, Zero-Drift, Precision Instrumentation Amplifier*. 2004. URL: https://www.analog.com/en/products/ad8230.html (visited on 12/11/2020).
[87] Maxim Integrated Products Inc. *MAX31865 – RTD-to-digital converter*. 2015. URL: https://datasheets.maximintegrated.com/en/ds/MAX31865.pdf (visited on 01/11/2021).
[88] C. D. Ghilani. Adjustment Computations: Spatial Data Analysis. Wiley, Hoboken, 2017. Chap. 12.
[89] T. Shimoda, K. Juhel, J.-P. Ampuero, J.-P. Montagner, and M. Barsuglia. Early earthquake detection capabilities of different types of future-generation gravity gradiometers. *Geophys J Int* 224, 533 (2021).
[90] D. Schlippert et al. Quantum Test of the Universality of Free Fall. *Phys Rev Lett* 112, 203002 (2014).
[91] M. A. Hohensee, H. Müller, and R. B. Wiringa. Equivalence Principle and Bound Kinetic Energy. *Phys Rev Lett* 111, 151102 (2013).
[92] G. Rosi et al. Quantum test of the equivalence principle for atoms in coherent superposition of internal energy states. *Nat Commun* 8, 15529 (2017).
[93] T. Kovachy et al. Quantum superposition at the half-metre scale. *Nature* 528, 530 (2015).
[94] B. Schrinksi, S. Nimmrichter, and K. Hornberger. Quantum-classical hypothesis tests in macroscopic matter-wave interferometry. *Phys Rev Research* 2, 033034 (2020).
[95] L. Hu, N. Poli, L. Salvi, and G. M. Tino. Atom Interferometry with the Sr Optical Clock Transition. *Phys Rev Lett* 119, 263601 (2017).
[96] N. Yu and M. Tinto. Gravitational wave detection with single-laser atom interferometers. *Gen Relat Gravit* 43, 1943 (2011).
[97] M. Zych, F. Costa, I. Pikovski, and Č. Brukner. Quantum interferometric visibility as a witness of general relativistic proper time. *Nat Commun* 2, 505 (2011).
[98] R. F. C. Vessot et al. Test of Relativistic Gravitation with a Space-Borne Hydrogen Maser. *Phys Rev Lett* 45, 2081 (1980).

[99] S. Loriani et al. Interference of Clocks: A Quantum Twin Paradox. *Sci Adv* 5, eaax8966 (2019).
[100] C. Ufrecht et al. Atom-interferometric test of the universality of gravitational redshift and free fall. *Phys Rev Research* 2, 043240 (2020).
[101] W. P. Schleich, D. M. Greenberger, and E. M. Rasel. Redshift Controversy in Atom Interferometry: Representation Dependence of the Origin of Phase Shift. *Phys Rev Lett* 110, 010401 (2013).

Acknowledgements

This thesis would not have been possible without the fantastic work of many remarkable scientists, dedicated managers, competent sales representatives, creative engineers, and skilled craftsmen. They shaped the scientific project, promoted their ideas to funding agencies, generously shared their scientific and technical knowledge, patiently advised on a wide range of topics, pushed the deadlines, found brilliant solutions to sometimes often badly-defined problems, transformed rough sketches into beautiful and highly functional pieces of hardware, and proved to be fantastic work partners. I would like to express my deepest gratitude to all the persons who, from everyday work to punctual advice have contributed to this work and the development of the Hannover VLBAI facility. In particular:

- Ernst Rasel, for offering me the chance to work on the VLBAI project and supervising my thesis. Thank you for your guidance and trust, in particular when developing new ideas and starting academic or industrial collaborations, as well as the fantastic opportunity to present our work at international conferences.
- Wolfgang Ertmer for inspiring and promoting this and many other projects in Hannover, and accepting to critically review this work.
- Markus Arndt for agreeing to examine this thesis and Hendrik Weimer for chairing the evaluation committee.
- Dennis Schlippert, who supervised the daily work on the experiments and provided skill, guidance, and the necessary confidence when making the most crucial decisions. Thank you for the autonomy you allowed and trust you expressed at all levels, from planning the cold-atoms experiment to organizing crane operations, as well as the good time on the many trips to Hägendorf, Berne, and Göttingen.
- Christian Schubert, for always providing expert support when dealing with fundamentals of atom interferometry and his accurate knowledge of the field.
- Present and past members of the VLBAI team. Thank you Christian M., Dorothee, Bob, and Klaus for the nice working atmosphere, your enthusiasm, the constructive and the less productive discussions, your immense help when handling the large-scale components, and accepting to suffer through the early years of the ARTIQ control system. Thank you Christian for starting the adventure with me. Thank you Dorothee for your optimistic realism and the spontaneous trip to Switzerland. Thank you Bob for bringing humor and great advancement to the Yb experiment, especially when I was too busy with the baseline hardware. Thank

you Klaus for your dedication and deploying plenty of new ideas in the Yb lab. Best wishes of success to Ali upon joining on this endeavor. Many thanks also to all the students who contributed to many projects, in particular Till, Thomas, Alice, and Luc.

- Matt Jaffe, who only spent two months in Hannover, but the great progress on the cavity looks like these were more!
- All the members of Ernst's group and the IQ in general for the friendly, supportive, and motivating working atmosphere.
- Manuel and Ludger for their patience and skill, giving substance to the geodetic part of the VLBAI vision. Thanks a lot for the crash course in applied gravimetry and the good stories during the long measurement campaigns.
- Kai-Martin for so generously sharing his knowledge, far exceeding the domain of the electronics workshop.
- The IQ's mechanical workshop, for manufacturing the space-ship Zeeman slower's frame, as well as many, many, other high-quality mechanical parts.
- The IQ, QUEST, and LUH central administrations for their tremendous help, in particular when organizing business trips or the experiment's finances. Many thanks notably to Ms. Göldner-Pauer, Ms. Thiele-Bode, Ms. Ohlendorf, Ms. Wiebking, and Mr. Barkow.
- Tobias and Alexander, for running the HITec building. Thanks for your support and flexibility when dealing with the sometimes crazy ideas we came up with.
- Daniel Penkert, for helping us optically contacting the mirrors of the Yb reference cavity.
- The entire team at IMEDCO around Urs Schläpfer and Mischa Widmer for taking the risk to design and build a unique magnetic shield and hosting us way beyond the initial agreement, always in a friendly and professional atmosphere.
- Peter Fierlinger and Stefan Stuiber, who were instrumental in the design and commissioning of the magnetic shield.
- Jens Voigt and Katharina Rolfs from PTB Berlin for the valuable advice in magnetic testing and the opportunity to use the BMSR-2 facility.
- The teams at the companies who helped us engineering, producing, and installing the instrument's key components. In particular Heinz Berlin, Aljo, Pfeiffer Vacuum, Innoseis, Dederding, and Nolte Autokrane.
- The cheese evening group, for accepting to eat some not always very successful (cheese-based) dishes.
- Daniel, Dennis, Dennis, and Magdalena, for the great rock-climbing and bouldering sessions.
- Toutes celles et ceux qui m'ont soutenu, offert d'autres perspectives que le travail, partagé des repas, randonnées, jeux de société, voyages, de chouettes moments de vie. Merci !

List of publications

1. **E. Wodey**, R. J. Rengelink, C. Meiners, E. M. Rasel, and D. Schlippert
   A robust, high-flux source of laser-cooled ytterbium atoms
   Journal of Physics B: Atomic, Molecular, and Optical Physics 54, 035301, 2021
   DOI: 10.1088/1361-6455/abd2d1

2. M. Schilling, **E. Wodey**, L. Timmen, D. Tell, K. H. Zipfel, D. Schlippert, C. Schubert, E. M. Rasel, and J. Müller
   Gravity field modelling for the Hannover 10 m atom interferometer
   Journal of Geodesy 94, 122, 2020
   DOI: 10.1007/s00190-020-01451-y

3. L. L. Richardson, A. Rajagopalan, H. Albers, C. Meiners, D. Nath, C. Schubert, D. Tell, **E. Wodey**, S. Abend, M. Gersemann, W. Ertmer, E. M. Rasel, D. Schlippert, M. Mehmet, L. Kumanchik, L. Colmenero, R. Spannagel, C. Braxmaier, and F. Guzmán
   Optomechanical resonator-enhanced atom interferometry
   Communications Physics 3, 208, 2020
   DOI: 10.1038/s42005-020-00473-4

4. **E. Wodey**, D. Tell, E. M. Rasel, D. Schlippert, R. Baur, U. Kissling, B. Kölliker, M. Lorenz, M. Marrer, U. Schläpfer, M. Widmer, C. Ufrecht, S. Stuiber, and P. Fierlinger
   A scalable high-performance magnetic shield for Very Long Baseline Atom Interferometry
   Review of Scientific Instruments 91, 035117, 2020
   DOI: 10.1063/1.5141340

5. S. Loriani, A. Friedrich, C. Ufrecht, F. Di Pumpo, S. Kleinert, S. Abend, N. Gaaloul, C. Meiners, C. Schubert, D. Tell, **E. Wodey**, M. Zych, W. Ertmer, A. Roura, D. Schlippert, W. P. Schleich, E. M. Rasel, and E. Giese
   Interference of Clocks: A Quantum Twin Paradox
   Science Advances 5, eaax8966, 2019
   DOI: 10.1126/sciadv.aax8966

6. D. Schlippert, C. Meiners, R. J. Rengelink, C. Schubert, D. Tell, **E. Wodey**, K. H. Zipfel, W. Ertmer, and E. M. Rasel
Matter-Wave Interferometry for Inertial Sensing and Tests of Fundamental Physics
In: Proceedings of the Eighth Meeting on CPT and Lorentz Symmetry, Indiana U. Bloomington (USA) 12 – 16 May 2019
DOI: 10.1142/9789811213984_0010

7. E. M. Rasel, D. Schlippert, and **E. Wodey**
Der VLBAI-Teststand : Ein Fallturm für Atome
In: Unimagazin 3/4, Leibniz Universität Hannover, 2018
DOI: 10.15488/5133

8. C. Jarlov, **E. Wodey**, A. Lyasota, M. Calic, P. Gallo, B. Dwir, A. Rudra, and E. Kapon
Effect of Pure Dephasing and Phonon Scattering on the Coupling of Semiconductor Quantum Dots to Optical Cavities
Physical Review Letters 117, 076801, 2016
DOI: 10.1103/PhysRevLett.117.076801

9. M. Andia, **E. Wodey**, F. Biraben, P. Cladé, and S. Guellati-Khélifa
Bloch oscillations in an optical lattice generated by a laser source based on a fiber amplifier: decoherence effects due to amplified spontaneous emission
Journal of the Optical Society of America B 32, 1028, 2015
DOI: 10.1364/josab.32.001038